RESEARCH ARTICLE

Open Access

Open Data

Open Code

***Correspondence:**
paul.blondiaux@inrae.fr

Dynamic sensitivity analysis of a mathematical model describing the effect of the macroalgae *Asparagopsis taxiformis* on rumen fermentation and methane production under *in vitro* continuous conditions

Paul Blondiaux[1*], Tristan Senga Kiessé[2], Maguy Eugène[3] and Rafael Muñoz-Tamayo[1]

[1] Université Paris-Saclay, INRAE, AgroParisTech, UMR Modélisation Systémique Appliquée aux Ruminants, 91120, Palaiseau, France.

[2] INRAE, UMR SAS, Institut Agro, 35000 Rennes, France.

[3] INRAE, UCA, VetAgro Sup, UMR Herbivores 1213, 63122 Saint-Genès-Champanelle, France.

Abstract

Ruminants plays an important role in global warming by emitting enteric methane (CH_4) through the degradation of feeds by the rumen microbiota. To better understand the dynamics fermentation outputs, including methane and volatile fatty acids (VFA) production, mathematical models have been developed. Sensitivity analysis (SA) methods quantify the contribution of model input parameters (IP) to the variation of an output variable of interest. In animal science, SA are usually conducted in static condition. In this work, we hypothesized that including the dynamic aspect of the rumen fermentation to SA can be useful to inform on optimal experimental conditions aimed at quantifying the key mechanisms driving CH_4 and VFA production. Accordingly, the objective of this work was to conduct a dynamic SA of a rumen fermentation model under *in vitro* continuous conditions (close to the real *in vivo* conditions). Our model case study integrates the effect of the macroalgae *Asparagopsis taxiformis* (AT) on the fermentation. AT has been identified as a potent CH_4 inhibitor via the presence of bromoform, an anti-methanogenic compound. We implemented two SA methods. We computed Shapley effects and full and independent Sobol indices over time for quantifying the contribution of 16 IPs to CH_4 (mol/h) and VFA (mol/l) variation. Our approach allows to discriminate the 3 contribution types of an IP to output variable variation (individual, via the interactions and via the dependence/correlation). We studied three diet scenarios accounting for several doses of AT relative to Dry Matter (DM): control (0% DM of AT), low treatment (LT: 0.25% DM of AT) and high treatment (HT: 0.50% DM of AT). Shapley effects revealed that hydrogen (H_2) utilizers microbial group via its Monod H_2 affinity constant highly contributed (> 50%) to CH_4 variation with a constant dynamic over time for control and LT. A shift on the impact of microbial pathways driving CH_4 variation was revealed for HT. IPs associated with the kinetic of bromoform utilization and with the factor modeling the direct effect of bromoform on methanogenesis were identified as influential on CH_4 variation in the middle of fermentation. Whereas, VFA variation for the 3 diet scenarios was mainly explained by the kinetic of fibers degradation, showing a high constant contribution (> 30%) over time. In addition, the Sobol indices indicated that interactions between IPs played a role on CH_4 variation, which was not the case of VFA variation. However, these results are dependent on the way interactions are represented in the model. The simulations computed for the SA were also used to analyze prediction uncertainty. It was related to the dynamic of dry matter intake (DMI, g/h), increasing during the high intake activity periods and decreasing when the intake activity was low. Moreover, CH_4 (mol/h) simulations showed a larger variability than VFA simulations, suggesting that the reduction of the uncertainty of IPs describing the activity of the H_2 utilizers microbial group is a promising lead to reduce the overall model uncertainty. Our results highlighted the dynamic nature of the influence of metabolic pathways on CH_4 productions under an anti-methanogenic treatment. SA tools can be further exploited to design optimal experiments studying rumen fermentation and CH_4 mitigation strategies. These optimal experiments would be useful to build robust models that can guide the development of sustainable nutrition strategies.

1. Introduction

Reducing methane (CH_4) emissions from ruminants is an important challenge for the livestock sector. At the global level, these emissions are responsible of 14.5% of total greenhouse gases (GHG) from human activity sources (Fao, 2017), highlighting the important role of ruminants in global warming. In France, CH_4 emissions represented 48% of total GHG emissions from agricultural sector in 2021 (CITEPA, 2023). In this context, Masson-Delmotte et al. (2019) highlighted that decreasing agricultural CH_4 emissions by 11 to 30% of the 2010 level by 2030 and by 24 to 47% by 2050 must be achieved to meet the 1.5 °C target of the Paris Agreement. In addition, Arndt et al. (2022) indicated that some mitigation strategies scenarios may allow to meet the 1.5 °C target by 2030. However, this study also highlighted that it was not possible to meet this target by 2050 considering that expected increase in milk and meat demand will lead to an increase of GHG emissions.

Ruminants produce CH_4 during the degradation and fermentation of feeds (Morgavi et al., 2010; Beauchemin et al., 2020). The fermentation process is done by a complex community of microbes inhabiting the forestomach (rumen) of ruminants. These microbial community (rumen microbiota) are constituted by members of bacteria, archaea, fungi and protozoa. The products of fermentation include volatile fatty acids (VFA), which are useful compounds for the animal, and CH_4. The development of mitigation actions aiming to reduce the enteric CH_4 production without affecting animal performance and welfare is a crucial challenge for the field (Hristov et al., 2013; Pellerin et al., 2013; Torres et al., 2020).

To better understand rumen fermentation and help design such strategies, mechanistic models describing the dynamic process of the rumen fermentation were developed. A synthesis of the characteristics of these models is presented by Tedeschi et al. (2014). Among these, the 3 most popular dynamic mechanistic models of rumen fermentation are: Molly (Baldwin et al., 1987), Dijkstra et al. (1992) and Karoline (Danfær et al., 2006).

These dynamic models involved numerous input parameters (IPs) representing biological and physical processes. The complexity of such models raises the need to investigate model behaviour, including the various relationships among IPs and outputs. To address this need, sensitivity analysis (SA) methods were used to assess the contribution of IP variability on the variability of the output of interest, identifying IPs which contribute the most to model predictions variability from those having a negligible effect (Faivre et al., 2013; Iooss and Lemaître, 2015; Saltelli et al., 2008, 2005).

In animal science, SA is usually conducted on mechanistic models with the main objective of reducing their complexity and identifying which IPs requires more accurate measurements for reducing output uncertainty. For instance, Huhtanen et al. (2015) and van Lingen et al. (2019) used linear regressions for describing the effects of some parameters on the variation of daily scale enteric CH_4 emissions in the Karoline model and an updated version of the Dijkstra model, respectively. In addition, Morales et al. (2021) and Dougherty et al. (2017) computed the Sobol indices (Sobol, 1993) for quantifying the effects of 19 and 20 parameters on several output variables of the Molly and AusBeef (Nagorcka et al., 2000) models, respectively.

Morales et al. (2021) did not consider the CH_4 production among the 27 output variables studied, while VFAs were considered. Dougherty et al. (2017) considered the daily CH_4 production in the output variables. In both studies, uniform distributions were set for exploring parameter variability. Recently, Merk et al. (2023) adapted and calibrated the model of Muñoz-Tamayo et al. (2021) to represent experimental data from the *in vitro* RUSITEC study of Roque et al. (2019), which aimed at evaluating the effect of the macroalgae *Asparagosis taxiformis* (AT) on CH_4 production and rumen microbiota. Authors used a Sobol based approach for identifying key parameters associated to microbial pathways driving CH_4 production with and without the presence of AT.

Although different SA approaches were applied to mechanistic models in the literature, several aspects still need to be explored. One aspect is the dynamic characteristic of the rumen fermentation. Most of the studies mentioned above explored sensitivity of mechanistic models at a single time point or under steady state conditions. However, the impact of IPs might vary over time, since the rumen is a dynamic system. Capturing this dynamic effect is of relevance to better understand rumen function (Morgavi et al., 2023) and to design CH_4 mitigation strategies. To our knowledge, SA has not been applied in dynamic conditions for studying CH_4 and VFA predictions of rumen models. Other aspect to explore in mechanistic models is the nature of the contribution of the IPs to model outputs by identifying: 1) the effect due to the IPs alone, 2) the effect due to the interactions between the IPs and 3) the effect due to the dependence or correlation between the IPs. Some references mentioned above implemented a method differentiating some effects of the contribution of an IP to output (individual, interaction and dependence/correlation). Dougherty et al. (2017) computed first-order and total Sobol indices (Homma and Saltelli, 1996), quantifying the individual and interaction effects of IPs. Whereas, van Lingen et al. (2019) concluded that there was no interaction between parameter covariates when studying the variation of daily scale enteric CH_4 emissions. The quantification of the contribution due to the dependence/correlation between the IPs has been an important research activity of the applied mathematics field for several years now (Kucherenko et al., 2012; Mara et al., 2015; Xu and Zdzislaw Gertner, 2008). Not all the SA methods are able to identify these 3 effects, conducting to biases in the estimated sensitivity indices.

The aim of this work was to conduct a complete SA of a dynamic model of rumen fermentation under *in vitro* continuous conditions accounting for the effect of AT on the fermentation and CH_4 production. The model studied extends previous developments of Muñoz-Tamayo et al. (2016, 2021). The AT macroalgae has been identified as a potent CH_4 inhibitor (Machado et al., 2014) with reported *in vivo* reductions of CH_4 emissions over 80% and 98% in beef cattle (Kinley et al., 2020; Roque et al., 2021). The original model (Muñoz-Tamayo et al., 2021) represented the fermentation under batch conditions. We extended the model to account for continuous condition which aimed at providing a model closer to the *in vivo* conditions. Also, the *in silico* framework in which SA is conducted was used to analyze the uncertainty associated with the outputs of interest over time. This work also addresses the limitations pointed out by Tedeschi (2021) in the evaluation process of the model in Muñoz-Tamayo et

al. (2021), which did not include SA to assess the impact of model parameters on the model outputs.

2. Methods

2.1. Presentation of the mechanistic model

2.1.1. Phenomena representation

The structure of the rumen fermentation model used in this study is determined by the representation of two phenomena namely the flow transport and microbial fermentation. The first is a biochemical and physical phenomenon describing the transport fluxes in the system, here represented as a reactor. The second is a biological phenomenon describing the microbial fermentation of feeds.

The system studied is displayed in Figure 1.

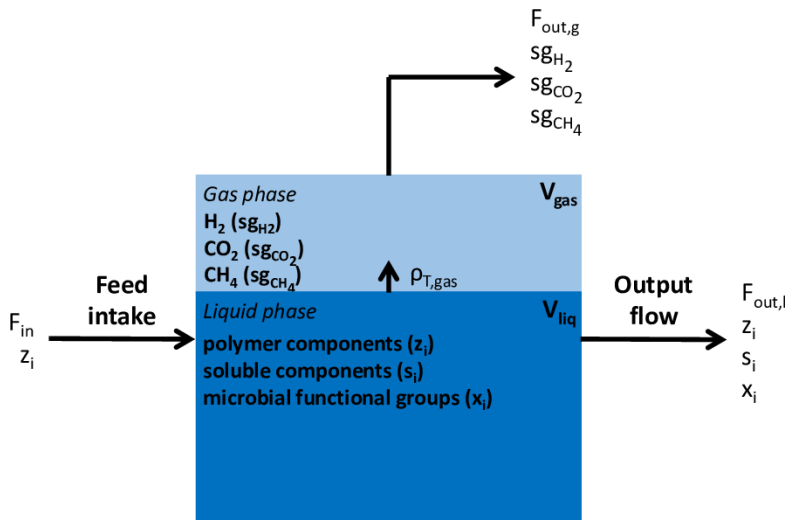

Figure 1. Representation of the *in vitro* continuous system.

This system is represented as a reactor system similar to engineering anaerobic digestion reactors (Batstone et al., 2002). It represents a rumen simulation technique (RUSITEC) system on a daily scale. Characteristics of the simulated RUSITEC system were taken from the setting used in Belanche et al., 2017. The total volume of the system was set to 0.8 L with a separation of 0.74 L in liquid phase (V_l) and 0.06 L in gas phase (V_g). The daily total dry matter intake (DMI) was of 11.25 g/d. In our model, the DMI was set as a dynamic equation determined by the number of feed distributions (n_r). For the feed distribution j, the *DMI* kinetics follows

$$DMI(\mathrm{t}) = \frac{\lambda_{n_j}.DM_{total}}{n_r}.\mathrm{e}^{-k\mathrm{t}} \quad (1)$$

Where DM_{total} is the total DMI ingested in one day (g), λ_{n_j} is the fraction of DM_{total} supplied in the distribution j and k (h^{-1}) is the intake kinetic rate. DM_{total} was set to 11.25 g supplied in two feed distributions ($n_r = 2$). We set the first feed distribution to account for 70% of the

total DM ($\lambda_{n_1} = 0.7$). This configuration provides a daily DMI composed of 2 distributions with a significantly greater amount of dry matter (DM) ingested during the first intake and a medium intake kinetic (Figure 2).

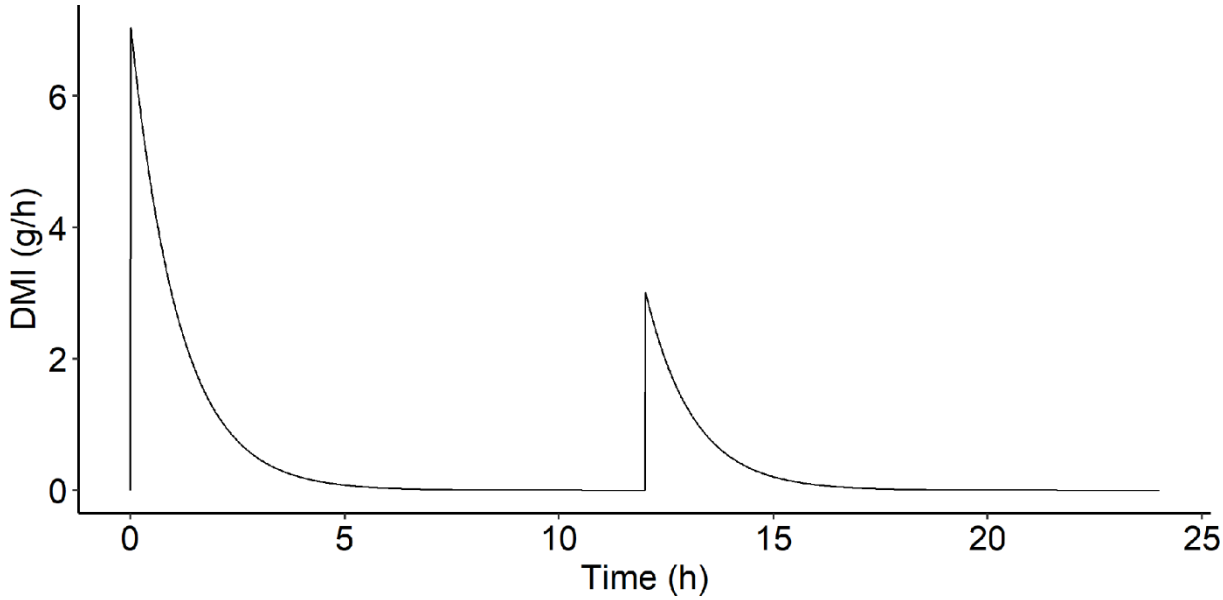

Figure 2. Dry matter intake (DMI, g/h) over time (h) simulated for one day with $DM_{total} = 11.25$ g, $n_r = 2$, $\lambda_{n_1} = 0.7$ and $\mathrm{k} = 0.015$.

The feed intake constitutes the input flux of the system. The feed is degraded by the rumen microbiota, leading to the production of several components in liquid and gas phase. Polymer components, soluble components and microbial functional groups are the components in liquid phase, and hydrogen, carbon dioxide and CH_4 are the components in gas phase. Chemical compounds leave the system in liquid and gas phases as shown in Figure 1.
The representation of the fermentation process is displayed in Figure 3.

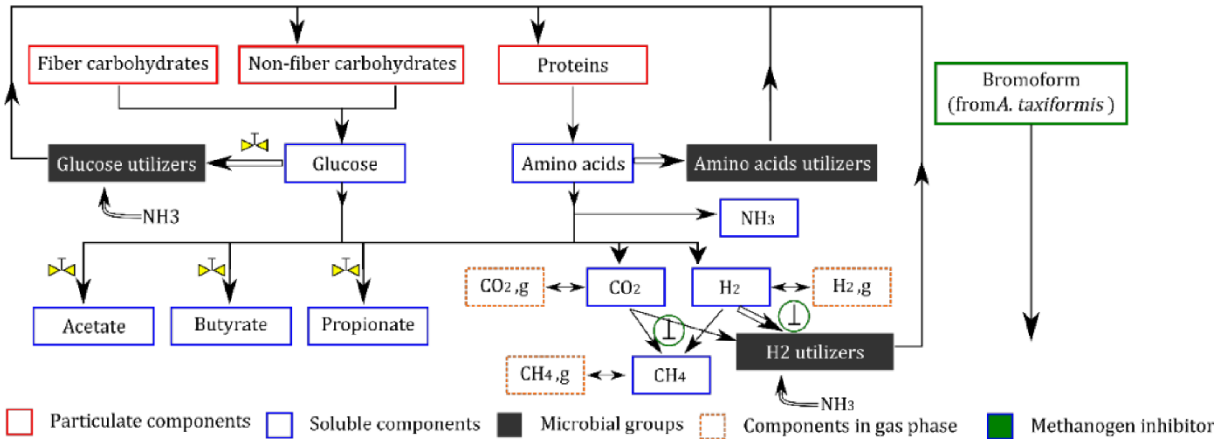

Figure 3. Representation of the *in vitro* rumen fermentation from Muñoz-Tamayo et al., 2021 model.

Biochemical assumptions used to describe the fermentation are detailed in Muñoz-Tamayo et al. (2021, 2016). The main assumptions are: 1) 3 polymer components are considered in the rumen: fiber carbohydrates, non-fiber carbohydrates and proteins, 2) hydrolysis of polymer components releases glucose (for fibers and non-fibers) and amino acids (for proteins), constituting 2 of the 3 soluble limiting substrates available in the rumen. The last soluble limiting substrate available is hydrogen, 3) the rumen microbiota is represented by 3 microbial functional groups (glucose utilizers, amino acids utilizers and hydrogen utilizers) determined by the microbial utilization of the 3 soluble limiting substrates in the fermentation pathway, 4) the utilization of the soluble substrates by biological pathways is done towards 2 mechanisms: product formation and microbial growth, 5) acetate, propionate and butyrate are the only VFA produced from the fermentation and 6) CH_4, carbon dioxide and hydrogen are the gas outputs of the fermentation.

The inclusion of bromoform as the inhibitor compound of AT impacted the fermentation *via* 2 mechanisms. First, the bromoform has a direct inhibition of the growth rate of methanogens, resulting in a CH_4 production reduction and hydrogen accumulation. Second, the bromoform affects indirectly, through the hydrogen accumulation, the flux allocation towards VFA production, as hydrogen exerts control on this component (Mosey, 1983).

The resulting model comprises 19 state variables corresponding to 19 biochemical component concentrations in liquid and gas phases.

2.1.2. Model equations

Model state variables are defined as $\boldsymbol{\xi} = (\mathbf{z}, \mathbf{s}, \mathbf{x}, \mathbf{s_g})$, where $\mathbf{z} = (z_{\mathrm{ndf}}, z_{\mathrm{nsc}}, z_{\mathrm{pro}})$ is the vector of concentrations of the polymer components (neutral detergent fiber, non-structural carbohydrates and proteins; g/L), $\mathbf{s} = (s_{\mathrm{su}}, s_{\mathrm{aa}}, s_{\mathrm{ac}}, s_{\mathrm{bu}}, s_{\mathrm{pr}}, s_{\mathrm{IN}}, s_{\mathrm{IC}}, s_{\mathrm{H_2}}, s_{\mathrm{CH_4}}, s_{\mathrm{br}})$ is the vector of concentrations of the soluble components (sugars, amino acids, acetate, butyrate, propionate, inorganic nitrogen, inorganic carbon, hydrogen, CH_4 and bromoform; mol/L), $\mathbf{x} = (x_{\mathrm{su}}, x_{\mathrm{aa}}, x_{\mathrm{H_2}})$ is the vector of concentrations of the microbial functional groups (sugars utilizers, amino acids utilizers and hydrogen utilizers; mol/L) ,$\mathbf{s_g} = (s_{\mathrm{g,CO_2}}, s_{\mathrm{g,H_2}}, s_{\mathrm{g,CH_4}})$ is the vector of concentrations in gas phase (carbon dioxide, hydrogen and CH_4; mol/L). The polymer components include an input flux in their equation and all the components are associated with an output flux in liquid or gas phase. The input flux (g/(Lh)) of polymer components is described as

$$F_{i,\mathrm{in}} = \frac{w_i \,.\, DMI}{V_{\mathrm{l}}} \tag{2}$$

where w_i is the fraction of polymer component i in the diet of the animal, DMI is the DM intake (g/h) with a total DM of 11.25 g split in two feed distributions along the day with the first distribution accounts for 70% of the total DM, and V_{l} the volume in liquid phase of the rumen (L).

The output flux in liquid phase (g/(Lh) for polymer components and mol/(Lh) for soluble and microbial functional groups components) is described as

$$F_{i,\mathrm{out,l}} = D \,.\, z_i, \text{for polymer components} \quad (3)$$

$$F_{i,\mathrm{out,l}} = D \,.\, s_i, \text{for soluble components} \quad (4)$$

$$F_{i,\mathrm{out,l}} = D \,.\, x_\mathrm{i}, \text{for microbial functional groups} \quad (5)$$

where D is the dilution rate (D = 0.035 h^{-1}, Bayat et al., 2011), z_i is the concentration of polymer component i, s_i is the concentration of soluble component i and x_i is the concentration of microbial functional group i.

The output flux in gas phase (mol/(Lh)) is described as

$$F_{i,\mathrm{out,g}} = \frac{q_\mathrm{g} \,.\, s_{\mathrm{g},i}}{V_\mathrm{g}} \quad (6)$$

where $q_\mathrm{g} = \frac{R\,.T\,.V_\mathrm{l}\,.(\rho_{\mathrm{T,H_2}}+\rho_{\mathrm{T,CO_2}}+\rho_{\mathrm{T,CH_4}})}{P-p_{\mathrm{H_2O}}}$ is the output flow of gas phase (L/h) wit R the ideal gas constant (barL/(molK)), T the temperature of the rumen (K), $\rho_{\mathrm{T,H_2}}$, $\rho_{\mathrm{T,CO_2}}$ and $\rho_{\mathrm{T,CH_4}}$ the liquid-gas transfer phenomena rates of hydrogen, carbon dioxide and CH_4 (mol/(Lh)), respectively, P the total pressure (bars) and $p_{\mathrm{H_2O}}$ the partial pressure of water vapor (bar). $s_{\mathrm{g},i}$ is the concentration of component i in gas phase (mol/L) and V_g is the volume in gas phase of the rumen (L).

Model equations are derived from mass balance equations described below.

For polymer components

$$\frac{\mathrm{d}z_\mathrm{ndf}}{\mathrm{dt}} = F_\mathrm{ndf,in} - \rho_\mathrm{ndf} - F_\mathrm{ndf,out,l} \quad (7)$$

$$\frac{\mathrm{d}z_\mathrm{nsc}}{\mathrm{dt}} = F_\mathrm{nsc,in} - \rho_\mathrm{nsc} + (f_\mathrm{ch,x}\,.\,w_\mathrm{mb}).\left(\rho_{x_\mathrm{su}} + \rho_{x_\mathrm{aa}} + \rho_{x_{\mathrm{H_2}}}\right) - F_\mathrm{nsc,out,l} \quad (8)$$

$$\frac{\mathrm{d}z_\mathrm{pro}}{\mathrm{dt}} = F_\mathrm{pro,in} - \rho_\mathrm{pro} + \left(f_\mathrm{pro,x}\,.\,w_\mathrm{mb}\right).\left(\rho_{x_\mathrm{su}} + \rho_{x_\mathrm{aa}} + \rho_{x_{\mathrm{H_2}}}\right) - F_\mathrm{pro,out,l} \quad (9)$$

where $F_\mathrm{ndf,in}$, $F_\mathrm{nsc,in}$ and$F_\mathrm{pro,in}$ are the input fluxes of neutral detergent fiber, non-structural carbohydrates and proteins (g/(Lh)), respectively. ρ_ndf, ρ_nsc and ρ_pro are the hydrolysis rate functions of polymer components (g/(Lh)), indicating the kinetic of hydrolysis of polymer components. These functions are described as

$$\rho_i = k_{\mathrm{hyd},i}.\,z_i \quad (10)$$

With $k_{\mathrm{hyd},i}$ the hydrolysis rate constant (h^{-1}) and z_i the concentration of polymer component i (g/L). $F_\mathrm{ndf,out}$, $F_\mathrm{nsc,out}$ and $F_\mathrm{pro,out}$ are the output fluxes of polymer components (g/(Lh)). The middle part of equations (8) and (9) represents the recycling of dead microbial cells where $f_\mathrm{ch,x}$, $f_\mathrm{pro,x}$ are the fractions of carbohydrates and proteins of the biomass, w_mb is the molecular weight of microbial cells (g/mol) and $\rho_{x_\mathrm{su}} = k_\mathrm{d}\,.\,x_\mathrm{su}$, $\rho_{x_\mathrm{aa}} = k_\mathrm{d}\,.\,x_\mathrm{aa}$, $\rho_{x_{\mathrm{H_2}}} = k_\mathrm{d}\,.\,x_{\mathrm{H_2}}$ are the cell death rate of sugars utilizers, amino acids utilizers and hydrogen utilizers (mol/(Lh)) with k_d the rate of dead of microbial cells (h^{-1}).

For soluble components

$$\frac{\mathrm{d}s_\mathrm{su}}{\mathrm{dt}} = \frac{\rho_\mathrm{ndf}}{w_\mathrm{su}} + \frac{\rho_\mathrm{nsc}}{w_\mathrm{su}} - \rho_\mathrm{su} - F_\mathrm{su,out,l} \quad (11)$$

$$\frac{\mathrm{d}s_\mathrm{aa}}{\mathrm{dt}} = \frac{\rho_\mathrm{pro}}{w_\mathrm{aa}} - \rho_\mathrm{aa} - F_\mathrm{aa,out,l} \quad (12)$$

$$\frac{\mathrm{d}s_{\mathrm{H_2}}}{\mathrm{dt}} = Y_{\mathrm{H_2,su}} \cdot \rho_{\mathrm{su}} + Y_{\mathrm{H_2,aa}} \cdot \rho_{\mathrm{aa}} - \rho_{\mathrm{H_2}} - \rho_{\mathrm{T,H_2}} - F_{\mathrm{H_2,out,l}} \tag{13}$$

$$\frac{\mathrm{d}s_{\mathrm{ac}}}{\mathrm{dt}} = Y_{\mathrm{ac,su}} \cdot \rho_{\mathrm{su}} + Y_{\mathrm{ac,aa}} \cdot \rho_{\mathrm{aa}} - F_{\mathrm{ac,out,l}} \tag{14}$$

$$\frac{\mathrm{d}s_{\mathrm{bu}}}{\mathrm{dt}} = Y_{\mathrm{bu,su}} \cdot \rho_{\mathrm{su}} + Y_{\mathrm{bu,aa}} \cdot \rho_{\mathrm{aa}} - F_{\mathrm{bu,out,l}} \tag{15}$$

$$\frac{\mathrm{d}s_{\mathrm{pr}}}{\mathrm{dt}} = Y_{\mathrm{pr,su}} \cdot \rho_{\mathrm{su}} + Y_{\mathrm{pr,aa}} \cdot \rho_{\mathrm{aa}} - F_{\mathrm{pr,out,l}} \tag{16}$$

$$\frac{\mathrm{d}s_{\mathrm{IN}}}{\mathrm{dt}} = Y_{\mathrm{IN,su}} \cdot \rho_{\mathrm{su}} + Y_{\mathrm{IN,aa}} \cdot \rho_{\mathrm{aa}} + Y_{\mathrm{IN,H_2}} \cdot \rho_{\mathrm{H_2}} - F_{\mathrm{IN,out,l}} \tag{17}$$

$$\frac{\mathrm{d}s_{\mathrm{IC}}}{\mathrm{dt}} = Y_{\mathrm{IC,su}} \cdot \rho_{\mathrm{su}} + Y_{\mathrm{IC,aa}} \cdot \rho_{\mathrm{aa}} + Y_{\mathrm{IC,H_2}} \cdot \rho_{\mathrm{H_2}} - \rho_{\mathrm{T,CO_2}} - F_{\mathrm{IC,out,l}} \tag{18}$$

$$\frac{\mathrm{d}s_{\mathrm{CH_4}}}{\mathrm{dt}} = Y_{\mathrm{CH_4,H_2}} \cdot \rho_{\mathrm{H_2}} - \rho_{\mathrm{T,CH_4}} - F_{\mathrm{CH_4,out,l}} \tag{19}$$

Let us detail how the amino acids are produced and used by the biological pathways in the fermentation process. Equation (12) indicates that amino acids are produced (positive sign in the equation) from the degradation of proteins, occurring with the kinetic rate ρ_{pro} (g/L h), which is divided by the molecular weight of the amino acids w_{aa} (g/mol). Moreover, amino acids are utilized (negative sign in the equation) by the biological pathways during the fermentation with the kinetic rate ρ_{aa} (mol/Lh). The kinetic rate ρ_{aa} is a function indicating the kinetic of utilization of amino acids during the fermentation and is described as

$$\rho_{\mathrm{aa}} = \frac{k_{\mathrm{m,aa}} . s_{\mathrm{aa}} . x_{\mathrm{aa}}}{K_{\mathrm{S,aa}} + s_{\mathrm{aa}}} \tag{20}$$

With $k_{\mathrm{m,aa}}$ the maximum specific utilization rate constant of amino acids (mol substrate/(mol biomass h)), s_{aa} the concentration of amino acids (mol/L), x_{aa} the concentration of amino acids-utilizing microbes (mol/L) and $K_{\mathrm{S,aa}}$ the Monod affinity constant associated with the utilization of amino acids (mol/L). $F_{\mathrm{aa,out}}$ is the output flux of amino acids concentration (mol/(Lh)). Then, further in the fermentation, amino acids are utilized by the specific microbial functional group x_{aa} and contributed to the production of hydrogen (Equation 13), VFA (Equations 14, 15, 16), inorganic nitrogen (Equation 17) and inorganic carbon (Equation 18) with a stoichiometry represented by the yield factors $Y_{\mathrm{H_2,aa}}$, $Y_{\mathrm{ac,aa}}$, $Y_{\mathrm{bu,aa}}$, $Y_{\mathrm{pr,aa}}$, $Y_{\mathrm{IN,aa}}$ and $Y_{\mathrm{IC,aa}}$, respectively. These components are also produced from glucose metabolism. In the last step of the biochemical conversion cascade, inorganic nitrogen and inorganic carbon are utilized during the reaction of hydrogen utilization in liquid phase with the kinetic rate function $\rho_{\mathrm{H_2}}$ (mol/L h), described similarly as Equation (20). An additional term (I_{br}) is included to represent the inhibition effect of bromoform on the hydrogen utilizers (methanogens) as detailed later on. Hydrogen in liquid phase is also associated with a transfer phenomenon with hydrogen in gas phase given by the rate $\rho_{\mathrm{T,H_2}}$ (mol/(Lh)). This liquid-gas transfer phenomenon also concerns carbon dioxide with the rate $\rho_{\mathrm{T,CO_2}}$ (mol/(Lh)) and CH_4 (Equation 19) with the rate $\rho_{\mathrm{T,CH_4}}$(mol/(Lh)). The general equation of the liquid-gas transfer rate is described as

$$\rho_{\mathrm{T},i} = k_{\mathrm{L}}\mathrm{a}.\left(s_i - K_{\mathrm{H},i}.p_{\mathrm{g},i}\right) \tag{21}$$

With $k_{\mathrm{L}}\mathrm{a}$ the mass transfer coefficient (h^{-1}), s_i the concentration (mol/L), $K_{\mathrm{H},i}$ the Henry's law coefficient (M/bar) and $p_{\mathrm{g},i}$ the partial pressure (bars) of soluble component i.

Finally, CH_4 in liquid phase is produced using hydrogen in liquid phase with the stoichiometry $Y_{\mathrm{CH_4,H_2}}$.

For microbial functional groups

$$\frac{\mathrm{d}x_{\mathrm{su}}}{\mathrm{dt}} = Y_{\mathrm{su}} \cdot \rho_{\mathrm{su}} - \rho_{x_{\mathrm{su}}} - F_{x_{\mathrm{su}},\mathrm{out,l}} \tag{22}$$

$$\frac{\mathrm{d}x_{\mathrm{aa}}}{\mathrm{dt}} = Y_{\mathrm{aa}} \cdot \rho_{\mathrm{aa}} - \rho_{x_{\mathrm{aa}}} - F_{x_{\mathrm{aa}},\mathrm{out,l}} \tag{23}$$

$$\frac{\mathrm{d}x_{\mathrm{H_2}}}{\mathrm{dt}} = Y_{\mathrm{H_2}} \cdot \rho_{\mathrm{H_2}} - \rho_{x_{\mathrm{H_2}}} - F_{x_{\mathrm{H_2}},\mathrm{out,l}} \tag{24}$$

Microbial functional groups of glucose utilizers (Equation 22), amino acid utilizers (Equation 23) and hydrogen utilizers (Equation 24) are produced from their respective substrates with the yield factors Y_{su}, Y_{aa} and $Y_{\mathrm{H_2}}$, respectively.

For the gas phase

$$\frac{\mathrm{d}s_{\mathrm{g,CO_2}}}{\mathrm{dt}} = V_{\mathrm{l}} \cdot \frac{\rho_{\mathrm{T,CO_2}}}{V_{\mathrm{g}}} - F_{\mathrm{CO_2,out,g}} \tag{25}$$

$$\frac{\mathrm{d}s_{\mathrm{g,H_2}}}{\mathrm{dt}} = V_{\mathrm{l}} \cdot \frac{\rho_{\mathrm{T,H_2}}}{V_{\mathrm{g}}} - F_{\mathrm{H_2,out,g}} \tag{26}$$

$$\frac{\mathrm{d}s_{\mathrm{g,CH_4}}}{\mathrm{dt}} = V_{\mathrm{l}} \cdot \frac{\rho_{\mathrm{T,CH_4}}}{V_{\mathrm{g}}} - F_{\mathrm{CH_4,out,g}} \tag{27}$$

The dynamics of carbon dioxide (Equation 25), hydrogen (Equation 26) and CH_4 (Equation 27) in gas phase are driven by the liquid-gas transfer phenomena given by the rates $\rho_{\mathrm{T,CO_2}}$, $\rho_{\mathrm{T,H_2}}$ and $\rho_{\mathrm{T,CH_4}}$ (mol/(Lh)), respectively.

Model parameters were either set with values extracted from the literature (Batstone et al., 2002; Serment et al., 2016), set with values reported from *in vitro* study providing the experimental data (Chagas et al., 2019) or estimated using the maximum likelihood estimator as reported in Muñoz-Tamayo et al. (2021). In the present study, initial conditions of state variables were determined by running the model for 50 days without AT supply (control condition). The idea was to reach a quasi-steady state of the state variables. Values corresponding to the last time step simulated were selected as initial conditions of the model for the further analysis explained below.

2.1.3. Integration of the macroalgae *Asparagosis taxiformis*

The integration of bromoform contained in AT conducted to the incorporation of the 19th state variable representing the dynamic of bromoform concentration.

$$\frac{\mathrm{d}s_{\mathrm{br}}}{\mathrm{dt}} = F_{\mathrm{br,in}} - k_{\mathrm{br}} \cdot s_{\mathrm{br}} - F_{\mathrm{br,out}} \tag{28}$$

Where $F_{\mathrm{br,in}} = \frac{w_{\mathrm{br}} \cdot DMI}{V_{\mathrm{l}}}$ is the input flux of bromoform concentration (g/(Lh)) with w_{br} the fraction of bromoform in the diet of the animal. k_{br} corresponds to the kinetic rate of

bromoform utilization (h^{-1}) and $F_{\mathrm{br,out}} = D\,.\,s_{\mathrm{br}}$ is the output flux of bromoform concentration (g/(Lh)). The value of k_{br} was obtained from data reported in Romero et al. (2023b) .

The direct effect of bromoform on the CH_4 production is represented through the factor I_{br} (Equation 29) impacting the kinetic rate function of hydrogen utilization ($\rho_{\mathrm{H_2}}$). This factor is a function of the bromoform concentration and is modeled by a sigmoid shape. Whereas the indirect effect of bromoform on the flux allocation towards VFA production is represented through the flux allocation parameters λ, describing the 3 reactions driving flux allocation from glucose utilization to VFA production. λ_1, λ_2 and λ_3 indicates the molar fraction of glucose utilized to produce acetate, to produce propionate and to produce butyrate, respectively. They follow $\lambda_1 + \lambda_2 + \lambda_3 = 1$. λ_1 (Equation 30) and λ_2 (Equation 31) are represented by affine functions described below.

$$I_{\mathrm{br}} = 1 - \frac{1}{1 + \exp\left(-p_1.\left(s_{\mathrm{br}} + p_2\right)\right)} \tag{29}$$

With s_{br} the bromoform concentration (g/L) and p_1, p_2 the parameters of sigmoid function.

$$\lambda_1 = p_3 - p_4.p_{\mathrm{H_2}} \tag{30}$$

With $p_{\mathrm{H_2}}$ the hydrogen partial pressure (bars) and p_3, p_4 the parameters of affine function.

$$\lambda_2 = p_5 + p_6.p_{\mathrm{H_2}} \tag{31}$$

With $p_{\mathrm{H_2}}$ the hydrogen partial pressure (bars) and p_5, p_6 the parameters of affine function.

These factors are displayed in Figure 4.

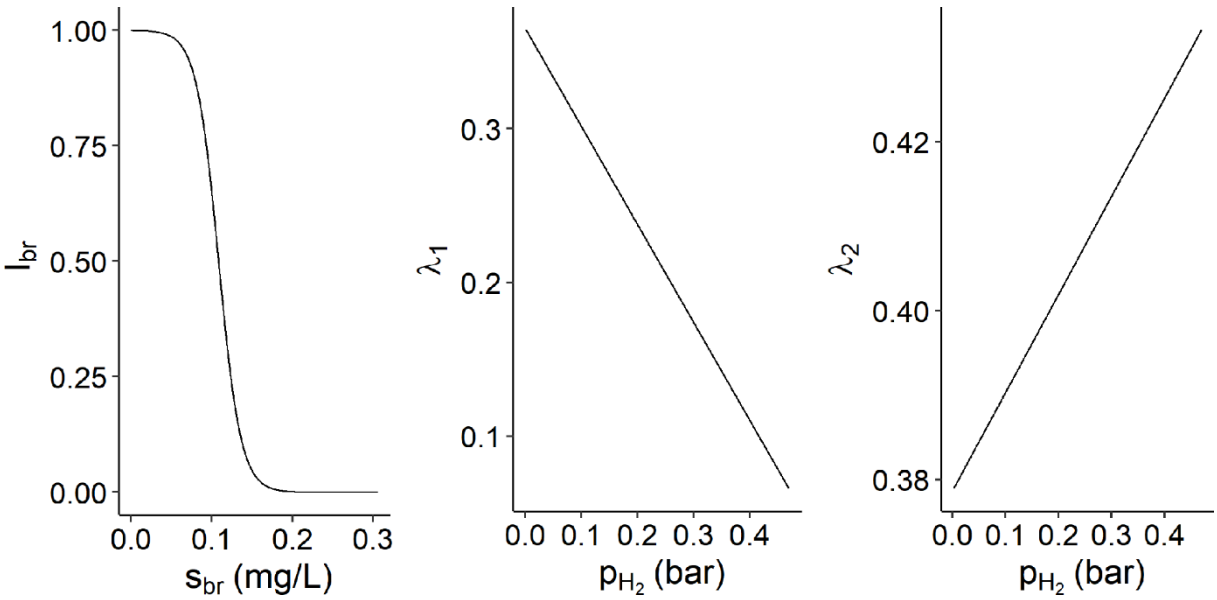

Figure 4. Representation of the direct effect of *Asparagosis taxiformis* on the methane production (I_{br}) against the bromoform concentration (s_{br}, mg/L), and of the indirect effect of *Asparagosis taxiformis*, through the hydrogen accumulation, on the flux allocation towards acetate production (λ_1) and propionate production (λ_2) against the hydrogen partial pressure ($\rho_{\mathrm{H_2}}$).

It should be noted that the model version of Muñoz-Tamayo et al. (2021) includes an inhibition factor of glucose utilization by hydrogen ($I_{\mathrm{H_2}}$). This factor was incorporated to account for the reduced production of VFA under AT supply observed in the experiments of Chagas et al. (2019). However, in the present study, we decided not to include this term. Some studies have shown that high doses of AT decrease total VFA both *in vitro* (Chagas et al., 2019; Kinley et al., 2016; Machado et al., 2016; Terry et al., 2023) and *in vivo* (Li et al., 2016; Stefenoni et al., 2021). However, in other studies the total VFA was unaffected by AT supplementation under *in vitro* (Romero et al., 2023b; Roque et al., 2019) and *in vivo* (Kinley et al., 2020) conditions. These discrepancies might be due to the variability of physical processing of the macroalgae (*e.g.*, drying, storage). The incorporation of the hydrogen inhibition factor was indeed challenged by Henk Van Lingen in the evaluation of the model in Muñoz-Tamayo et al., (2021) (Tedeschi, 2021). Accordingly, we acknowledge that this aspect requires further studies, and it is not then included in the present work. We then run again the calibration of the model without the $I_{\mathrm{H_2}}$ factor under batch conditions using the experimental data from Chagas et al. (2019) to estimate the parameters from equations (28-30). In the process, with the aim of model simplification, we set the allocation factors λ_1, λ_2 as linear functions of $p_{\mathrm{H_2}}$. The updated version of the model under batch conditions is available at Muñoz-Tamayo (2020).

Table 1. Stoichiometry matrix of biochemical reactions occurring during the rumen fermentation.

	Component → i	1	2	3	4	5	6	7	8	Kinetic rate
j	Microbial process ↓	z_{ndf}	z_{nsc}	z_{pro}	s_{su}	s_{aa}	$s_{\mathrm{H_2}}$	s_{ac}	s_{bu}	
1	Hydrolysis of NDF	-1			$1/w_{\mathrm{su}}$					ρ_{ndf}
1	Hydrolysis of NSC		-1		$1/w_{\mathrm{su}}$					ρ_{nsc}
2	Hydrolysis of proteins			-1		$1/w_{\mathrm{aa}}$				ρ_{pro}
3	Utilization of glucose				-1		$Y_{\mathrm{H_2,su}}$	$Y_{\mathrm{ac,su}}$	$Y_{\mathrm{bu,su}}$	ρ_{su}
4	Utilization of amino acids					-1	$Y_{\mathrm{H_2,aa}}$	$Y_{\mathrm{ac,aa}}$	$Y_{\mathrm{bu,aa}}$	ρ_{aa}
5	Utilization of hydrogen						-1			$\rho_{\mathrm{H_2}}$
6	Death of sugars utilizers		$f_{\mathrm{ch,x}} \cdot w_{\mathrm{mb}}$	$f_{\mathrm{pro,x}} \cdot w_{\mathrm{mb}}$						$\rho_{\mathrm{x_{su}}}$
7	Death of amino acids utilizers		$f_{\mathrm{ch,x}} \cdot w_{\mathrm{mb}}$	$f_{\mathrm{pro,x}} \cdot w_{\mathrm{mb}}$						$\rho_{\mathrm{x_{aa}}}$
8	Death of hydrogen utilizers		$f_{\mathrm{ch,x}} \cdot w_{\mathrm{mb}}$	$f_{\mathrm{pro,x}} \cdot w_{\mathrm{mb}}$						$\rho_{\mathrm{x_{H_2}}}$
9	Inhibition of bromoform									

	Component → i	9	10	11	12	13	14	15	16	Kinetic rate
j	Microbial process ↓	s_{pr}	s_{IN}	s_{IC}	$s_{\mathrm{CH_4}}$	x_{su}	x_{aa}	$x_{\mathrm{H_2}}$	s_{br}	
1	Hydrolysis of NDF									ρ_{ndf}
1	Hydrolysis of NSC									ρ_{nsc}
2	Hydrolysis of proteins									ρ_{pro}
3	Utilization of glucose	$Y_{\mathrm{pr,su}}$	$Y_{\mathrm{IN,su}}$	$Y_{\mathrm{IC,su}}$		Y_{su}				ρ_{su}
4	Utilization of amino acids	$Y_{\mathrm{pr,aa}}$	$Y_{\mathrm{IN,aa}}$	$Y_{\mathrm{IC,aa}}$			Y_{aa}			ρ_{aa}
5	Utilization of hydrogen		$Y_{\mathrm{IN,H_2}}$	$Y_{\mathrm{IC,H_2}}$	$Y_{\mathrm{CH_4,H_2}}$			Y_{H_2}		$\rho_{\mathrm{H_2}}$
6	Death of sugars utilizers					-1				$\rho_{x_{\mathrm{su}}}$
7	Death of amino acids utilizers						-1			$\rho_{x_{\mathrm{aa}}}$
8	Death of hydrogen utilizers							-1		$\rho_{x_{\mathrm{H_2}}}$
9	Inhibition of bromoform								$-k_{\mathrm{br}}$	

Table 2. Model parameters

	Definition	Unit	Value	Reference
Rates				
μ_j	Growth rate of the microbial group j	mol j/(L h)	$Y_j . \rho_j$	
ρ_j	Kinetic rate of microbial process j	Mol (or g) j/(L h)	$k_{\mathrm{m},j} \frac{s_j}{K_{\mathrm{s},j} + s_j} x_j$	
ρ_{x_j}	Death cell rate of microbes j	mol j/(L h)	$k_{\mathrm{d}} . x_{\mathrm{j}}$	
$\rho_{\mathrm{T},j}$	Liquid-gas transfer rate of component j	mol j/(L h)	$k_{\mathrm{L}}\mathrm{a}. (s_j - K_{\mathrm{H},j} . p_{\mathrm{gas},j})$	
Biochemical parameters				
λ_1	Molar fraction of the sugars utilized to produce acetate	mol/mol	$p_3 - p_4 . p_{\mathrm{H_2}}$	
λ_2	Molar fraction of the sugars utilized to produce acetate	mol/mol	$p_5 + p_6 . p_{\mathrm{H_2}}$	
λ_3	Molar fraction of the sugars utilized to produce acetate	mol/mol	$1 - (\lambda_1 + \lambda_2)$	
$\sigma_{\mathrm{ac,aa}}$	Stoichiometry coefficient of acetate production from amino acids utilization	mol/mol	0.67	
$\sigma_{\mathrm{bu,aa}}$	Stoichiometry coefficient of butyrate production from amino acids utilization	mol/mol	0.24	
$\sigma_{\mathrm{pr,aa}}$	Stoichiometry coefficient of propionate production from amino acids utilization	mol/mol	0.062	
$\sigma_{\mathrm{H_2,aa}}$	Stoichiometry coefficient of hydrogen production from amino acids utilization	mol/mol	0.82	
$\sigma_{\mathrm{IC,aa}}$	Stoichiometry coefficient of inorganic carbon production from amino acids utilization	mol/mol	0.88	
$f_{\mathrm{H_2}}$	Fraction of hydrogen utilized for product formation	mol/mol	$1 - 10 . Y_{\mathrm{H_2}}$	
f_{su}	Fraction of glucose utilized for product formation	mol/mol	$1 - \frac{5}{6} . Y_{\mathrm{su}}$	
$f_{\mathrm{ch,x}}$	Mass fraction of carbohydrates in the microbial cells	g/g	0.20	
$f_{\mathrm{pro,x}}$	Mass fraction of proteins in the microbial cells	g/g	0.55	
k_{br}	Kinetic rate constant of bromoform utilization	h^{-1}	0.095	Romero et al., 2023b
k_{d}	Death cell rate constant	h^{-1}	8.33e-04	
$k_{\mathrm{hyd,ndf}}$	Hydrolysis rate constant of cell wall carbohydrates	h^{-1}	0.024	
$k_{\mathrm{hyd,nsc}}$	Hydrolysis rate constant of non-structural carbohydrates	h^{-1}	0.06	
$k_{\mathrm{hyd,pro}}$	Hydrolysis rate constant of proteins	h^{-1}	0.09	
$k_{\mathrm{m,aa}}$	Maximum specific utilization rate constant of amino acids	mol /(mol h)	2.00	
$k_{\mathrm{m,H_2}}$	Maximum specific utilization rate constant of hydrogen	mol /(mol h)	16	
$k_{\mathrm{m,su}}$	Maximum specific utilization rate constant of glucose	mol /(mol h)	1.00	
$K_{\mathrm{s,aa}}$	Monod constant associated with the utilization of amino acids	mol/L	6.40e-03	
$K_{\mathrm{s,H_2}}$	Monod constant associated with the utilization of hydrogen	mol/L	5.84e-06	
$K_{\mathrm{s,su}}$	Monod constant associated with the utilization of glucose	mol/L	9.00e-03	

$K_{s,IN}$	Nitrogen limitation constant	mol/L	2.0e-04	
Y_{aa}	Microbial biomass yield factor of amino acids utilizers	mol/mol	0.31	
Y_{H_2}	Microbial biomass yield factor of hydrogen utilizers	mol/mol	0.006	
Y_{su}	Microbial biomass yield factor of glucose utilizers	mol/mol	0.16	
$Y_{ac,su}$	Yield factor of the acetate during utilization of glucose	mol/mol	$f_{su} . (2 . \lambda_1 + \frac{2}{3} . \lambda_2)$	
$Y_{bu,su}$	Yield factor of the butyrate during utilization of glucose	mol/mol	$f_{su} . (\lambda_3)$	
$Y_{pr,su}$	Yield factor of the propionate during utilization of glucose	mol/mol	$f_{su} . (\frac{4}{3} . \lambda_2)$	
$Y_{H_2,su}$	Yield factor of the hydrogen during utilization of glucose	mol/mol	$f_{su} . (4 . \lambda_1 + 2 . \lambda_3)$	
$Y_{IN,su}$	Yield factor of the inorganic nitrogen during utilization of glucose	mol/mol	$-Y_{su}$	
$Y_{IC,su}$	Yield factor of the inorganic carbon during utilization of glucose	mol/mol	$f_{su} . (2 . \lambda_1 + \frac{2}{3} . \lambda_2 + 2 . \lambda_3)$	
Y_{CH_4,H_2}	Yield factor of the methane during utilization of hydrogen	mol/mol	$f_{H_2} . (\frac{1}{4})$	
Y_{IC,H_2}	Yield factor of the inorganic carbon during utilization of hydrogen	mol/mol	$-(\left(\frac{1}{4}\right) . f_{H_2} + \left(\frac{5}{10}\right) . (1 - f_{H_2}))$	
Y_{IN,H_2}	Yield factor of the inorganic nitrogen during utilization of hydrogen	mol/mol	$-Y_{H_2}$	
$Y_{i,aa}$	Yield factor of the component i during utilization of amino acids	mol/mol	$(1 - Y_{aa}) . \sigma_{i,aa}$	
$Y_{IN,aa}$	Yield factor of the component inorganic nitrogen during utilization of amino acids	mol/mol	$N_{aa} - Y_{aa} . N_{mb}$	
Physicochemical parameters				
K_{a,CO_2}	Equilibrium constant of bicarbonate		5.13e-07	Batstone et al., 2002
K_{a,NH_4}	Equilibrium constant of ammonium		1.44e-09	Batstone et al., 2002
$K_{a,VFA}$	Equilibrium constant of VFA		1.74e-05	Batstone et al., 2002
K_w	Equilibrium coefficient of water		2.75e-14	Batstone et al., 2002
$k_L a$	Liquid-gas transfer constant	h^{-1}	8.33	
K_{H,CO_2}	Henry's law coefficient of carbon dioxide	M/bar	2.46e-02	Batstone et al., 2002
K_{H,CH_4}	Henry's law coefficient of methane	M/bar	1.10e-03	Batstone et al., 2002
K_{H,H_2}	Henry's law coefficient of hydrogen	M/bar	7.23e-04	Batstone et al., 2002
P	Pressure	bars	1.01325	Serment et al., 2016
T	Temperature	K	312.15	Serment et al., 2016
w_{aa}	Molecular weight of average amino acid	g/mol	134	Feedipedia
w_{ac}	Molecular weight of acetate	g/mol	60.05	Wikipedia
w_{bu}	Molecular weight of butyrate	g/mol	88.10	Wikipedia
w_{mb}	Molecular weight of microbial cells	g/mol	113	Batstone et al., 2002
w_{pr}	Molecular weight of propionate	g/mol	74.1	Wikipedia
w_{su}	Molecular weight of glucose	g/mol	180.16	Wikipedia

V_g	Volume of the gas phase	L	0.06	Belanche et al., 2017
V_l	Volume of the liquid phase	L	0.74	Belanche et al., 2017
Parameters of factors modelling the effect of bromoform on rumen fermentation				
p_1	Parameter of the factor I_{br} modelling the direct effect of bromoform on the CH_4 production		72551	
p_2	Parameter of the factor I_{br} modelling the direct effect of bromoform on the CH_4 production		-1.0837e-04	
p_3	Intercept of λ_1		0.3655	
p_4	Slope of λ_1		0.6371	
p_5	Intercept of λ_2		0.3787	
p_6	Slope of λ_2		0.1160	

2.2. Sensitivity analysis

We implemented two SA methods for quantifying the contribution of 16 IPs to the variability of 4 state variables of the mechanistic model described in the previous section. These 2 methods use a strong theoretical framework and provide easy-to-interpret sensitivity indices (SI). Moreover, the SI were computed over time allowing to study the dynamic of IP sensitivity during the fermentation. Thus, Shapley effects (Owen, 2014) and full and independent Sobol indices (Mara et al., 2015) were computed for quantifying the individual, interaction and dependence/correlation effects of an IP to the variability of an output. Although the model studied here provides no correlated or dependent IPs, these 2 methods were used to introduce a new SA method in the animal science field.

This work was done with the support of MESO@LR-Platform at the University of Montpellier, which was used to run the algorithms computing Shapley effects and Sobol indices. They were run using one node, 28 cores and 125 GB of RAM of memory.

2.2.1. Input parameters and output variables studied

State variables of the model considered as output variables of the SA were the rate of CH_4 production (in gas phase) ($q_{CH_4,g,out}$, mol/h) and VFA (acetate (s_{ac}), butyrate (s_{bu}) and propionate (s_{pr})) concentrations (mol/L). The model was runned for 4 days, similarly to the RUSITEC of Roque et al., (2019), and the SA was performed on the last day of simulation, from 72 to 96h with a time step of 1h.

Components constituting the model represent different factors associated to microbial pathways involved in *in vitro* rumen fermentation. These factors include polymer hydrolysis and microbial growth. The sensibility of hydrolysis rate constants associated with the 3 polymer components ($k_{hyd,ndf}$, $k_{hyd,nsc}$ and $k_{hyd,pro}$, h^{-1}) was studied for quantifying the impact of feed polymer hydrolysis on output variables of interest during the fermentation. In addition, the sensibility of maximum specific utilization rate constants ($k_{m,su}$, $k_{m,aa}$ and k_{m,H_2}, mol substrate/(mol biomass h)) and Monod constants ($K_{S,su}$, $K_{S,aa}$ and K_{S,H_2}, mol/L)

associated with the 3 microbial groups was studied for quantifying the impact of microbial growth on output variables of interest during the fermentation.

In addition to the IPs quantifying the impact of polymer components and microbial functional groups, IPs related to the effect of bromoform on the fermentation were considered. The kinetic rate constant of bromoform utilization (k_{br} , h^{-1}), quantifying the consumption of anti-methanogenic compounds, was added to the SA. Moreover, the parameters of sigmoid and affine functions associated with the factor representing the impact of bromoform on methanogens (I_{br} associated with parameters p_1 and p_2) and with the flux allocation from glucose utilization to VFA production (λ_1 associated with parameters p_3 and p_4, and λ_2 associated with parameters p_5 and p_6) were added to the SA. Therefore, in total, 16 IPs were considered.

The first step in SA was to set the variability space of IPs. To perform that, information about the variability of each IP was required. This information was available from 2 sources: data and expert knowledge (Table 3). Based on the low number of data available for each IP, uniform distributions were selected for quantifying hydrolysis rate constants, maximum specific utilization rate constants and Monod constants variability. Lower and upper bounds of uniform distributions were set by selecting the minimum and maximum values among all the references. Furthermore, the parameters associated with the effect of bromoform on the fermentation were not biological parameters and no data were available for modeling their variability. Therefore, a uniform distribution varying of ± 10% the baseline model parameter value was used for parameters p_1 to p_6.

Table 3. Variation range (minimum (min) and maximum (max)) and sources/references of uniform distributions used for exploring the variability of input parameters studied in the sensitivity analysis.

Parameter	Min	Max	References
$k_{\mathrm{hyd,ndf}}$	0.01	0.33	Chapoutot et al., 2010; Muñoz-Tamayo et al., 2016; van Lingen et al., 2019
$k_{\mathrm{hyd,nsc}}$	0.06	0.22	Muñoz-Tamayo et al., 2016; van Lingen et al., 2019
$k_{\mathrm{hyd,pro}}$	0.05	0.25	Muñoz-Tamayo et al., 2016; van Lingen et al., 2019
$k_{\mathrm{m,su}}$	0.94	4.33	Batstone et al., 2002; Muñoz-Tamayo et al., 2021, 2016
$K_{\mathrm{S,su}}$	1e-04	9e-03	Batstone et al., 2002; Muñoz-Tamayo et al., 2021, 2016
$k_{\mathrm{m,aa}}$	1	5	Batstone et al., 2002; Muñoz-Tamayo et al., 2021, 2016
$K_{\mathrm{S,aa}}$	3e-04	8e-03	Batstone et al., 2002; Muñoz-Tamayo et al., 2021, 2016
$k_{\mathrm{m,H_2}}$	12	25	Batstone et al., 2002; Muñoz-Tamayo et al., 2021, 2016
$K_{\mathrm{S,H_2}}$	1e-07	1e-05	Batstone et al., 2002; Muñoz-Tamayo et al., 2021, 2016
k_{br}	8.55e-02	1.04e-01	
p_1	6.52e+04	7.98e+04	
p_2	-1.19e-04	-9.75e-05	
p_3	0.33	0.40	
p_4	0.57	0.70	
p_5	0.34	0.42	

p_6	0.10	0.13

2.2.2. System characteristics, intake and dietary scenarios

The consideration of feed intake in the model studied allows to simulate dietary scenarios. The dietary scenarios studied in this work were set using data from an *in vitro* study assessing several dietary CH_4 mitigation strategies, including AT, on the fermentation (Chagas et al., 2019). This experiment tested the impact on CH_4 production of several doses of AT from 0 to 1% DM (containing 6.84 mg/g dry weight of bromoform) in the diet. The diet was composed of 38.7% DM of neutral detergent fiber, 39.7% DM of non-structural carbohydrates and 16% DM of crude proteins. We analyzed three simulation scenarios: A control treatment with 0% of AT, a low treatment with 0.25% of AT and a high treatment with 0.50% of AT (Figure 5).

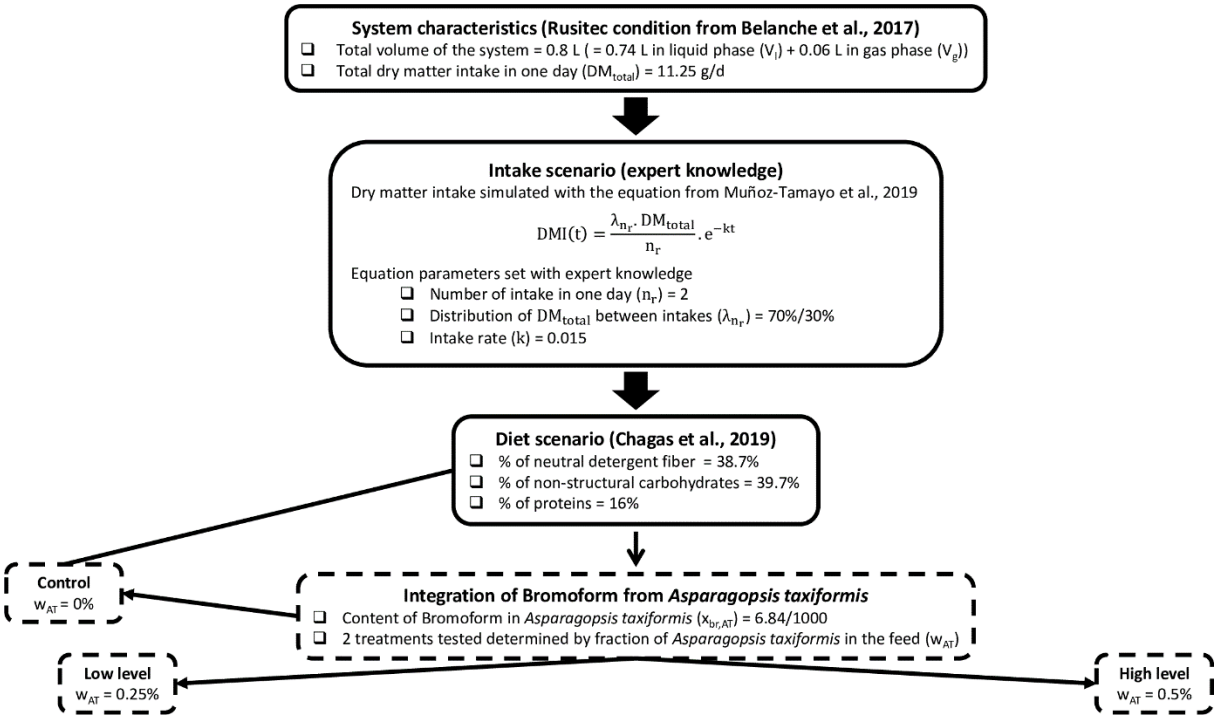

Figure 5. Summary of system characteristics, intake scenario and diet scenario simulated with the mechanistic model.

The initial condition of bromoform concentration was set to zero for all the 3 treatments.

2.2.3. Shapley effects

2.2.3.1. Definition

The first method implemented was the Shapley effects, which come from the field of cooperative game theory (Shapley, 1953). The Shapley effect of an IP X_i (Sh_i) measures the

part of variability of the output variable caused by the variability of X_i, and allocate to X_i a fair value regarding its individual contribution, its contribution due to interactions with other IPs and its contribution due to dependence/correlation with other IPs (Owen, 2014, Song et al., 2016). It is described as

$$Sh_i = \frac{1}{d} \sum_{u \subseteq -\{i\}} \binom{d-1}{|u|}^{-1} \left(\sum_{v \subseteq u+i} Var(E[Y|X_v]) - \sum_{v \subseteq u} Var(E[Y|X_v]) \right) \quad (32)$$

where d is the number of IPs, $u \subseteq \{1, \dots d\}$ is a subset of IPs, Y is the output variable and X is an IP.

2.2.3.2. Interpretation

The Shapley effects are condensed and easy-to-interpret. Their sum is equal to 1, allowing us to interpret them as the percentage of contribution of the IPs to output variability. Nevertheless, the distinction of individual, interaction and dependence/correlation effects are not possible. Each IP is associated with one value, integrating the 3 effects.

2.2.3.3. Numerical computation

Several methods are available for estimating the Shapley effects. In our study, the random permutation method was used (Song et al., 2016). This method provides a consistent estimation of the Shapley effects adapted in the case of numerous IPs (Iooss and Prieur, 2019). It is based on an alternative definition of the Shapley effects, expressing it in terms of all the possible IPs permutations (Castro et al., 2009). The cost of this method is $N_v + m(d-1)N_o N_i$ with N_v the sample size for estimating the output variance, m the number of permutations randomly sampled from the space of all the possible IP permutations, d the number of IPs considered, N_o the sample size for estimating the expectation and N_i the sample size for estimating the conditional variance. N_o and N_i were set at 1 and 3, respectively, as recommended in Song et al. (2016). In addition, $N_v = 1e04$ and $m = 1e04$ were considered, conducting to 460000 model evaluations. Estimation of the Shapley effects was performed using the R package “sensitivity” (Iooss et al., 2023).

2.2.4. Full and independent Sobol indices

2.2.4.1. Definition

Sobol indices (Sobol, 1993) are commonly used when performing SA. The first-order Sobol indice (S_i) of an IP X_i quantifies the individual contribution of X_i to output variability, based on the variance decomposition such as

$$S_i = \frac{Var(E[Y|X_i])}{Var(Y)} \quad (33)$$

where Y is the output variable and X_i is an IP. In addition, the total Sobol indice (T_i) (Homma and Saltelli, 1996) quantifies the contribution due to the interactions of X_i with other IPs such as

$$T_i = S_i + \sum_{j \neq i} S_{ij} + \sum_{j \neq i, k \neq i, j<k} S_{ijk} + \cdots \tag{34}$$

where S_i is the first-order Sobol indice of X_i, S_{ij} is the second-order Sobol indice of X_i quantifying the interactions between X_i and other IPs 2 by 2, S_{ijk} is the third-order Sobol indice of X_i quantifying the interactions between X_i and other IPs 3 by 3.

When dependence/correlation is present among the IPs, the variance decomposition is no longer applicable. Then, S_i and T_i are no longer computable. In this case, Mara et al. (2015) proposed Sobol indices allowing to quantify the contribution of an IP due to its dependence/correlation with other IPs by computing 4 SI:

- the full first-order and total Sobol indices (S_i^{full}, T_i^{full}) of an IP X_i integrate the dependence/correlation effects between X_i and other IPs;
- the independent first-order and total Sobol indices (S_i^{ind}, T_i^{ind}) of an IP X_i represent the effects of X_i that are not due to its dependence/correlation with other IPs.

2.2.4.2. Interpretation

Sobol indices of Mara et al. (2015) are interpreted in 2 steps:

a. T_i^{full} and T_i^{ind} are compared for quantifying the contribution of X_i due to its dependence/correlation effects.
    - The combination of a high T_i^{full} and a low T_i^{ind} indicates that X_i contributes to output variability only via its dependence/correlation with other IPs;
    - a high T_i^{ind} indicates that X_i contributes to output variability via its own variability and/or its interactions with other IPs;
    - a low T_i^{full} and T_i^{ind} indicates that X_i has no contribution on output variability
b. The second step of the interpretation is the comparison of S_i^{full} and T_i^{full} or S_i^{ind} and T_i^{ind}, depending on whether X_i contributes to output variability via its dependence/correlation with other IPs, for quantifying the contribution of X_i due to its interaction effects:
    - $T_i - S_i \approx 0$ indicates that X_i contributes to output variability via its own variability,
    - $T_i - S_i \gg 0$ indicates that X_i contributes to output variability via its interactions with other IPs.

2.2.4.3. Numerical computation

For estimating the 4 indices, IPs were sampled using the Sobol sequences, which were identified as providing a better stability for Sobol indices estimation (Blondiaux et al., 2022). 3000 simulations and 100 bootstrap replications using the Sobol (Sobol, 1993) and Saltelli

(Saltelli et al., 2008) estimators for computing first-order (S_i^{full} and S_i^{ind}) and total (T_i^{full} and T_i^{ind}) indices, respectively, were conducted with the R package "sensobol" (Puy et al., 2022), leading to 54000 model evaluations. Moreover, the estimation of conditional densities of the IPs is required for modelling their dependence structure. This estimation was conducted using a vine copula model.

In addition to the Shapley effects, the interpretation of S_i^{full}, T_i^{full}, S_i^{ind} and T_i^{ind} allows a distinction of the individual, interaction and dependence/correlation effects. Therefore, in our work, both methods were used in a complementary approach. First, the Shapley effects of the 16 IPs studied were computed for estimating their percentage of contribution, integrating the 3 effects, to the variability of output variables of interest. Second, the full and independent Sobol indices were computed for identifying what is the main source of contribution among these 3 effects.

2.3. Uncertainty analysis

SA provides a framework combining an IP sampling matrix, developed by randomly drawing values from IP probability distributions, to simulations of our 4 outputs of interest. This *in silico* framework was used for analyzing uncertainty associated with the simulations of CH_4, acetate, butyrate and propionate concentrations (mol/L). Similarly to SA, uncertainty associated with outputs of interest was studied dynamically by computing summary statistics (median, standard deviation (SD), and quantiles 10 and 90%) and the coefficient of variation (CV) of the output simulations at each time step.

3. Results

3.1. Analysis of the simulations of the mechanistic model

Figure 6 and Figure 7 display the dynamics of $q_{CH_4,g,out}$ and of VFA proportions, and propionate to acetate ratio of the 3 dietary scenarios (control: 0% of AT, low treatment: 0.25% of AT and high treatment: 0.50% of AT) for a 4 days simulation.

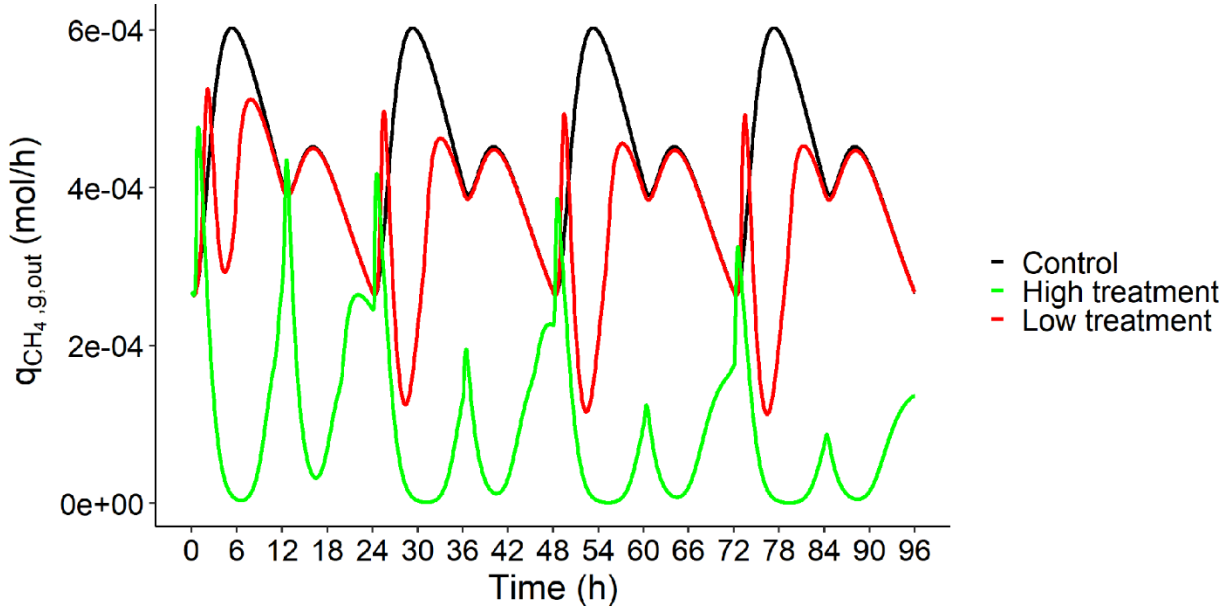

Figure 6. Rate of CH_4 production in gas phase ($q_{\mathrm{CH_4,g,out}}$, mol/h) over time (h) of the 3 dietary scenarios (control: 0% of *Asparagopsis taxiformis*, low treatment: 0.25% of *Asparagopsis taxiformis* and high treatment: 0.50% of *Asparagopsis taxiformis*) for a 4 days simulation.

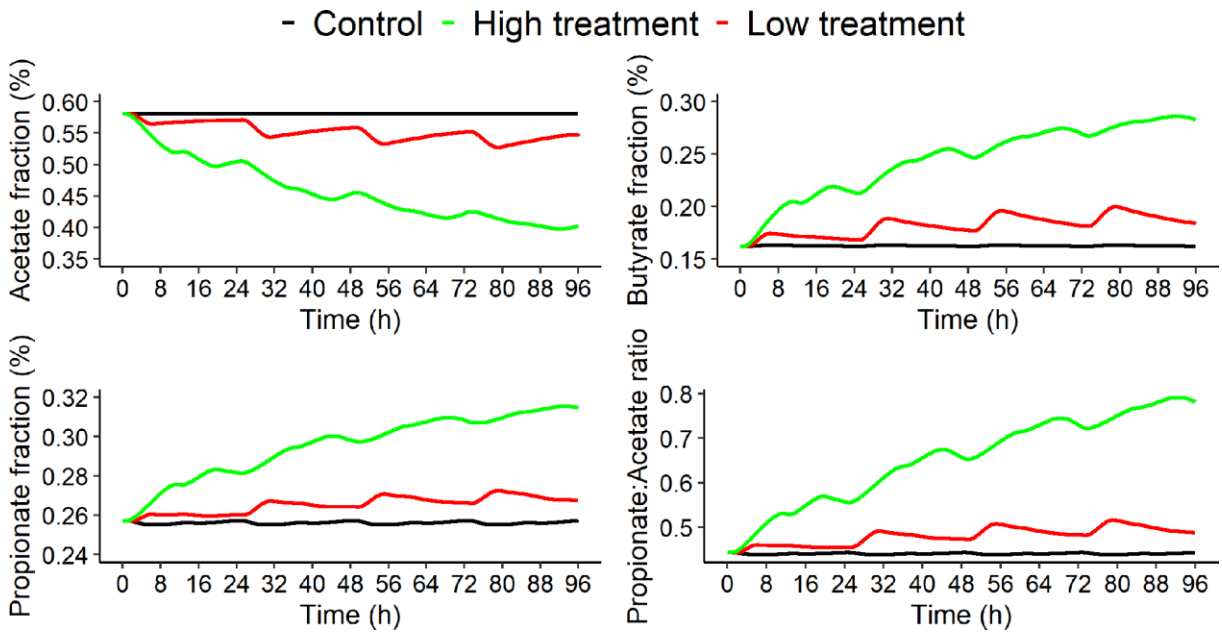

Figure 7. Acetate proportion (%), butyrate proportion (%), propionate proportion (%) and propionate to acetate ratio over time (h) of the 3 dietary scenarios (control: 0% of *Asparagopsis taxiformis*, low treatment: 0.25% of *Asparagopsis taxiformis* and high treatment: 0.50% of *Asparagopsis taxiformis*) for a 4 days simulation.

Increasing the dose of AT decreased $q_{\mathrm{CH_4,g,out}}$ with, at the end of the 4 days of simulations, a CH_4 (g/d) reduction of 17% between control and low AT treatment and of 78% between control and high AT treatment. This reduction increased from one day to the next with computed reductions of 9%, 14%, 16% and 17% between control and low AT treatment, and

of 65%, 72%, 75% and 78% between control and high AT treatment, from day 1 to 4, respectively.

The dynamic of VFA proportions showed that increasing AT dose in the diet decreased acetate proportion of 5% and 31% at the end of the fermentation between control, and low and high AT treatments, respectively. Whereas, butyrate and propionate proportions increased when increasing AT dose in the diet, with increases at the end of the fermentation (t = 96h) of 13% and 74% for butyrate proportion and of 4% and 22% for propionate proportion between control, and low and high AT treatments, respectively.

Propionate to acetate ratio was also associated with an increase of 10% between control and low AT treatment and of 76% between control and high AT treatment.

3.2. Sensitivity analysis

3.2.1. Shapley effects

Figure 8, Figure 9, Figure 10 and Figure 11 display the Shapley effects computed over time for the 4th day of simulation (from 72 to 96h) of $q_{\mathrm{CH_4,g,out}}$ (mol/h), s_{ac} (mol/L), s_{bu} (mol/L) and s_{pr} (mol/L), respectively, for the 3 dietary scenarios (control, low AT treatment and high AT treatment) studied. Only the IP associated with a contribution higher than 10% for at least one time step were displayed.

For some time steps, the computation led to negative indexes. In this case, the estimates were set to 0. These issues mainly concerned $q_{\mathrm{CH_4,g,out}}$ of the 2 AT treatments and were either due to the outliers in the variability explored in the simulations or to the lack of variability in the simulations for some time steps. The computational time for one dietary scenario was of 24h using the MESO@LR-Platform.

3.2.1.1. Rate of methane production

Figure 8 indicated that the microbial group of hydrogen utilizers, via the Monod affinity constant $K_{\mathrm{S,H_2}}$, contributed largely the most to the variability of $q_{\mathrm{CH_4,g,out}}$ over the fermentation for control and low AT treatment, explaining more than 50% of $q_{\mathrm{CH_4,g,out}}$ variation over time for both scenarios. The influence of this IP was also important for high AT treatment from 73 to 76h, from 87 to 89h and from 93 to 96h.

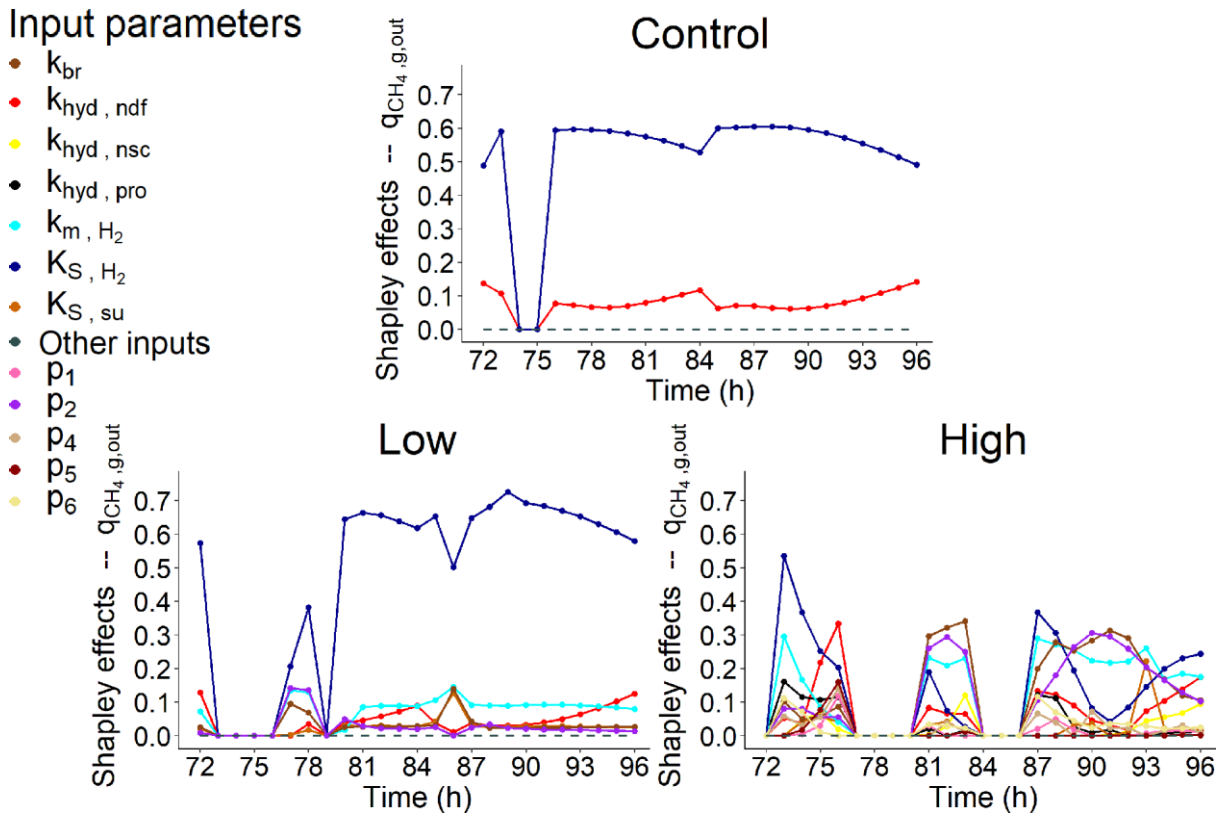

Figure 8. Shapley effects of the influential input parameters (*i.e*, parameters with a contribution higher than 10% for at least one time step) over time (h) computed for the 4th day of simulation of the rate of CH_4 production in gas phase ($q_{\mathrm{CH_4,g,out}}$, mol/h) for the 3 dietary scenarios (control: 0% of *Asparagopsis taxiformis*, low treatment: 0.25% of *Asparagopsis taxiformis* and high treatment: 0.50% of *Asparagopsis taxiformis*).

The other influential IP for control was related to fiber degradation via the hydrolysis rate constant $k_{\mathrm{hyd,ndf}}$, highlighting a contribution of c.a. 10% to $q_{\mathrm{CH_4,g,out}}$ variability over time. This IP showed a low influence (c.a. 10%) for low and high AT treatments.

Hydrogen utilizers microbial group also showed an influence via the maximum specific utilization rate constant $k_{\mathrm{m,H_2}}$ on $q_{\mathrm{CH_4,g,out}}$ variation of low and high AT treatments. This influence was low (c.a. 10%) for low AT treatment over the fermentation and was of c.a. 20% or higher at t = 73h, from 81 to 83h and from 87 to 96h for high AT treatment.

Moreover, for low and high AT treatments some IP associated with the factors modeling the effect of AT on the fermentation were highlighted. The IP p_2, which is related to the sigmoid function modelling the direct inhibition effect of AT on methanogenesis, showed a contribution to $q_{\mathrm{CH_4,g,out}}$ variability higher than 10% from 77 to 78h for low AT treatment and higher than 20% (most important contribution with the kinetic rate constant of bromoform utilization k_{br}) for high AT treatment. The IPs p_2 and k_{br} explained more than 50% of $q_{\mathrm{CH_4,g,out}}$ variability of high AT treatment at t = from 81 to 83h and from 88 to 92h. Their influence decreased at the end of the fermentation but was still higher than 20%. When comparing both IPs, k_{br} showed a slightly higher influence (< 10%) than p_2.

Finally, AT treatments highlighted the differences of the role of microbial pathways explaining the variation of $q_{\mathrm{CH_4,g,out}}$ when increasing the dose of AT. The IPs $k_{\mathrm{hyd,nsc}}$, $k_{\mathrm{hyd,pro}}$, $K_{\mathrm{S,su}}$, p_1, p_4, p_5 and p_6 showed a low but non-negligible influence (c.a. 10%) to $q_{\mathrm{CH_4,g,out}}$ variability for high AT treatment and were not influential for control and low AT treatment, except $K_{\mathrm{S,su}}$ which showed also a low influence (c.a. 10%) for low AT treatment.

3.2.1.2. Acetate concentration

Figure 9 showed that the fiber degradation via the hydrolysis rate constant $k_{\mathrm{hyd,ndf}}$ explained largely most of the variation of s_{ac} over the fermentation for control with a constant contribution higher than 60% over time. When increasing the dose of AT, the influence of $k_{\mathrm{hyd,ndf}}$ largely decreased while it was still the most influential IP. Its influence over time varied from 29 to 42% for low AT treatment and from 26 to 37% for high AT treatment.

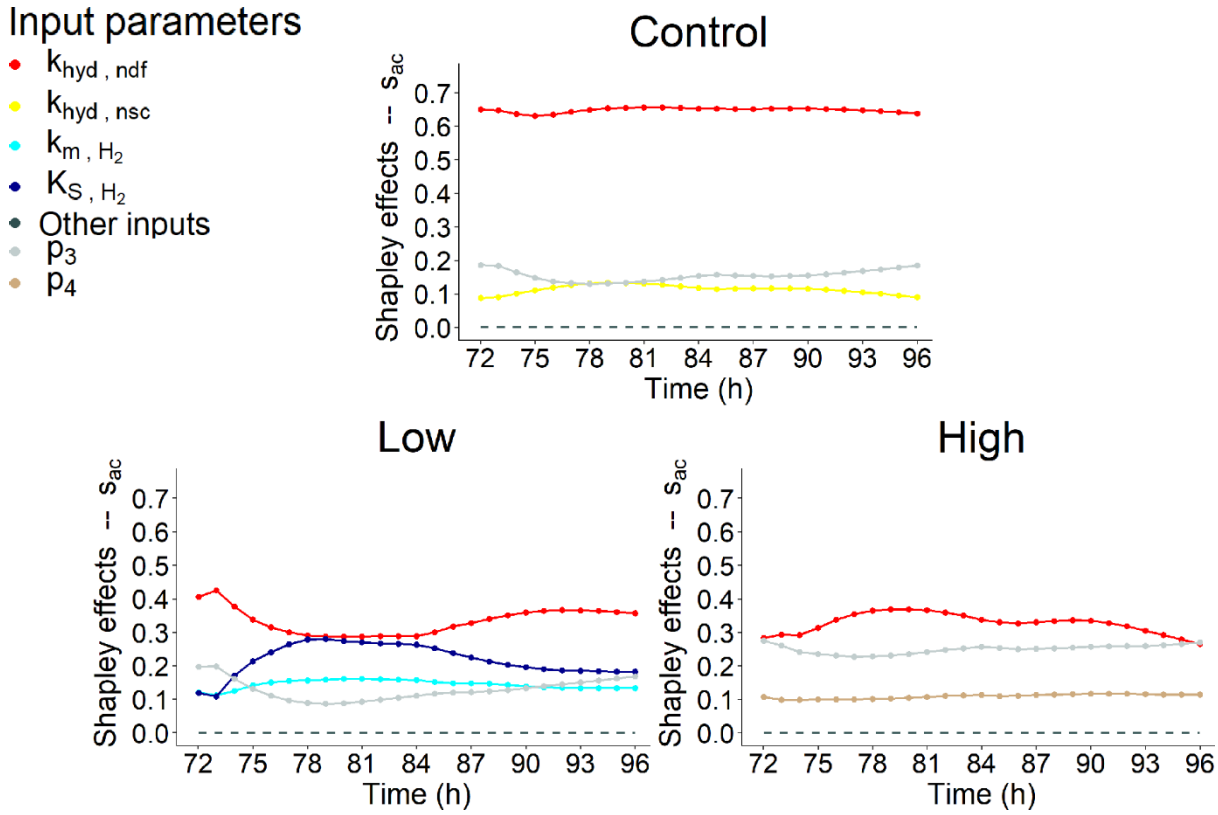

Figure 9. Shapley effects of the influential input parameters (i.e; parameters with a contribution higher than 10% for at least one time step) over time (h) computed for the 4th day of simulation of the acetate concentration (s_{ac}, mol/L) for the 3 dietary scenarios (control: 0% of *Asparagopsis taxiformis*, low treatment: 0.25% of *Asparagopsis taxiformis* and high treatment: 0.50% of *Asparagopsis taxiformis*).

The other influential IPs for Control were p_3, which was the intercept of the factor modeling the flux allocation from glucose utilization to acetate production in the rumen fermentation (λ_1), and $k_{\mathrm{hyd,nsc}}$, which was associated with the degradation of non-fiber compounds (Sh_{p_3}

and $\mathrm{Sh}_{k_{\mathrm{hyd,nsc}}}$ varying from 13 to 19%). The IP $k_{\mathrm{hyd,nsc}}$ was non-influential for AT treatments. Whereas, p_3 was associated with a non-negligible influence (< 20%) for low AT treatment, while it was more important (Sh_{p_3} varying from 23 to 27%) for high AT treatment, which was similar to $k_{\mathrm{hyd,ndf}}$ contribution from 72 to 74h and 93 to 96 h.

The microbial group of hydrogen utilizers, via the Monod constant $K_{\mathrm{S,H_2}}$ and the maximum specific utilization rate constant $k_{\mathrm{m,H_2}}$, contributed to s_{ac} variability for low AT treatment. This influence was mainly due to $K_{\mathrm{S,H_2}}$, being the second most influential IP from t = 74h to the end of the fermentation with a contribution varying from 17 to 27% over this period of time. $k_{\mathrm{m,H_2}}$was associated with a low contribution varying from 11 to 16% over the fermentation. The factor λ_1 was also represented via its slope p_4 with a constant low contribution (c.a. 10%) to s_{ac} variability over time for high AT treatment.

3.2.1.3. Butyrate concentration

Similarly to s_{ac}, the fiber degradation via the hydrolysis rate constant $k_{\mathrm{hyd,ndf}}$ was the most influential IP to s_{bu} variability over the fermentation for control and AT treatments (Figure 10). Its influence increased when increasing the dose of AT, varying from 34 to 42% for control, from 34 to 43% for low AT treatment and from 54 to 62% for high AT treatment over time.

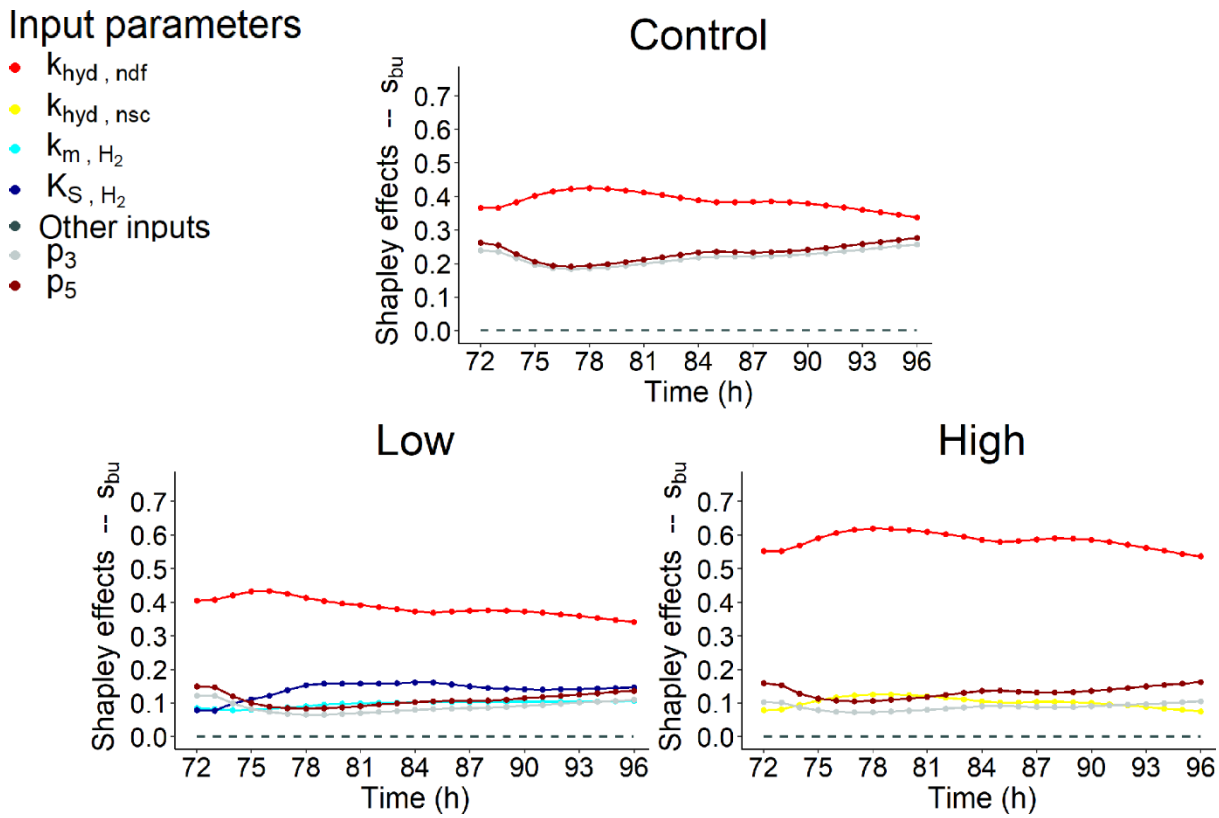

Figure 10. Shapley effects of the influential input parameters (i.e; parameters with a contribution higher than 10% for at least one time step) over time (h) computed for the 4th day of simulation of the butyrate concentration (s_{bu}, mol/L) for the 3 dietary scenarios (control: 0% of *Asparagopsis taxiformis*, low treatment: 0.25% of *Asparagopsis taxiformis* and high treatment: 0.50% of *Asparagopsis taxiformis*).

Intercepts of the factors modeling the flux allocation from glucose utilization to acetate and propionate production in the rumen fermentation (p_3 associated with λ_1 and p_5 associated with λ_2, respectively) were the other influential IPs for the 3 dietary scenarios with a similar contribution over time. The contribution of p_3 and p_5 to s_{bu} variability decreased when increasing the dose of AT. The contribution of p_3 and p_5 varied from c.a. 18 to 28% for control, 6 to 15% for low AT treatment and 7 to 16% for high AT treatment, respectively.

The microbial group of hydrogen utilizers, via the Monod constant $K_{\mathrm{S,H_2}}$ and the maximum specific utilization rate constant $k_{\mathrm{m,H_2}}$, slightly contributed to s_{bu} variability of the low AT treatment, similarly to s_{ac}. The contribution of $k_{\mathrm{m,H_2}}$ over the fermentation was low (c.a. 10%), while the contribution of $K_{\mathrm{S,H_2}}$ was higher, explaining a maximum of 16% of the variation of s_{bu} (second most influential IP).

The non-fiber degradation via the hydrolysis rate constant $k_{\mathrm{hyd,nsc}}$ slightly contributed (c.a. 10%) to s_{bu} variability over time of the high AT treatment.

3.2.1.4. Proprionate concentration

The variation of s_{pr} for the 3 dietary scenarios was mainly due to the contributions of 3 IPs (Figure 11).

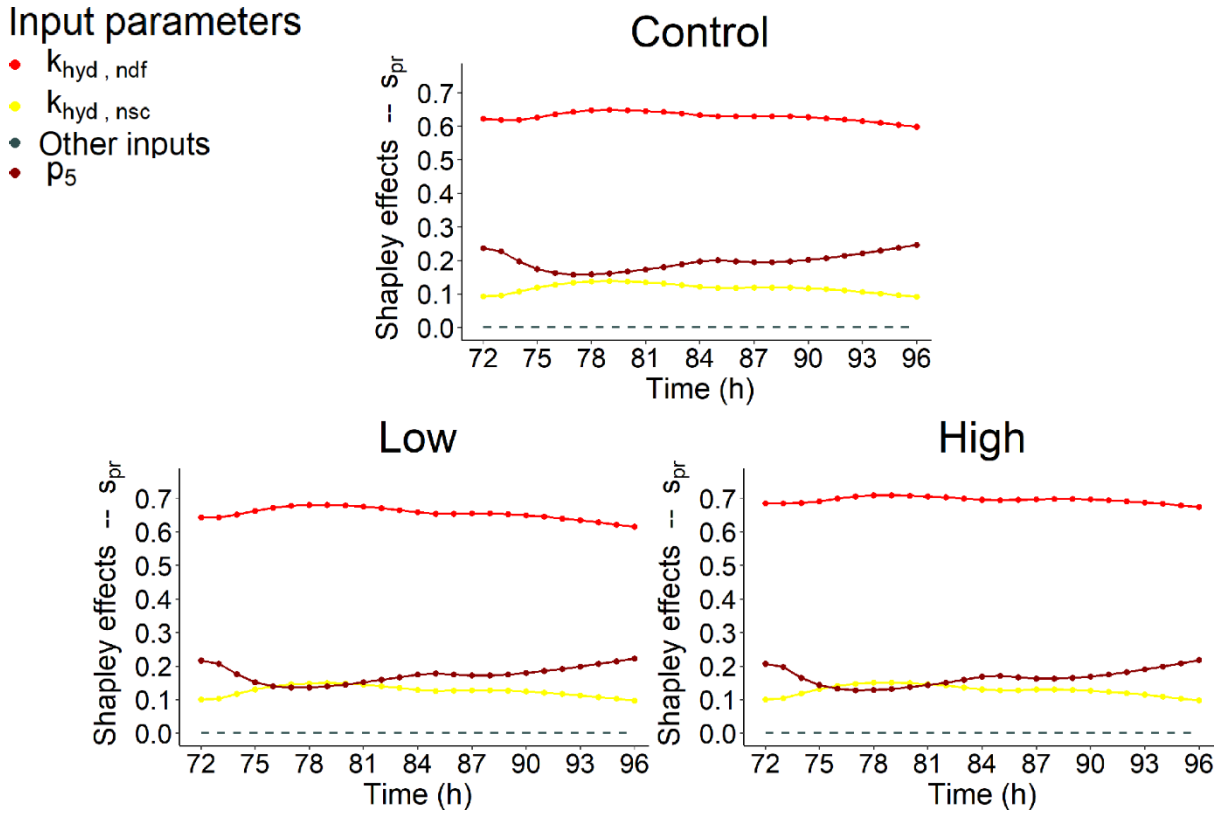

Figure 11. Shapley effects of the influential input parameters (i.e; parameters with a contribution higher than 10% for at least one time step) over time (h) computed for the 4th day of simulation of the propionate concentration (s_{pr}, mol/L) for the 3 dietary scenarios (control: 0% of *Asparagopsis taxiformis*, low treatment: 0.25% of *Asparagopsis taxiformis* and high treatment: 0.50% of *Asparagopsis taxiformis*).

This result was different from those obtained for the other output variables where new influential IPs were highlighted from a dietary scenario to another. Similarly to s_{ac} and s_{bu}, the fiber degradation via the hydrolysis rate constant $k_{\mathrm{hyd,ndf}}$ was the most influential IP to s_{pr} variability over the fermentation for control and AT treatments. Its influence increased when increasing the dose of AT, varying from 60 to 65% for control, from 61 to 68% for low AT treatment and from 67 to 71% for high AT treatment over time.

The other influential IPs were, by order of contribution, the intercept of the factor modeling the flux allocation from glucose utilization to propionate production in the rumen fermentation (p_5 associated with λ_2) and the non-fiber degradation IP $k_{\mathrm{hyd,nsc}}$. The contribution of p_5 slightly decreased when increasing the dose of AT with an average contribution over time of 20% for control, 17% for low AT and 16% for high AT. Whereas, the contribution of $k_{\mathrm{hyd,nsc}}$ was similar between the 3 dietary scenarios.

3.2.2. Full and independent Sobol indices

Similarly to the Shapley effects, the full and independent Sobol indices of the 16 IPs were computed over time, considering the 4th day of simulation, for the 4 output variables and 3 dietary scenarios studied. These indices were computed in addition to the Shapley effects for identifying the nature of the contribution of the IPs to output variable variation. The computational time for one dietary scenario was of 5h using the MESO@LR-Platform.

Since the model is associated with independent IPs, the difference between $\mathrm{T_i^{full}}$ and $\mathrm{T_i^{ind}}$ was systematically close to 0 for all the IPs, output variables and dietary scenarios studied, indicating that the contribution of IPs to output variable variation were not due to the dependence or correlation between IPs.

3.2.2.1. Rate of methane production

The full and independent Sobol indices were displayed only for $q_{\mathrm{CH_4,g,out}}$ (mol/h) (Figure 12).

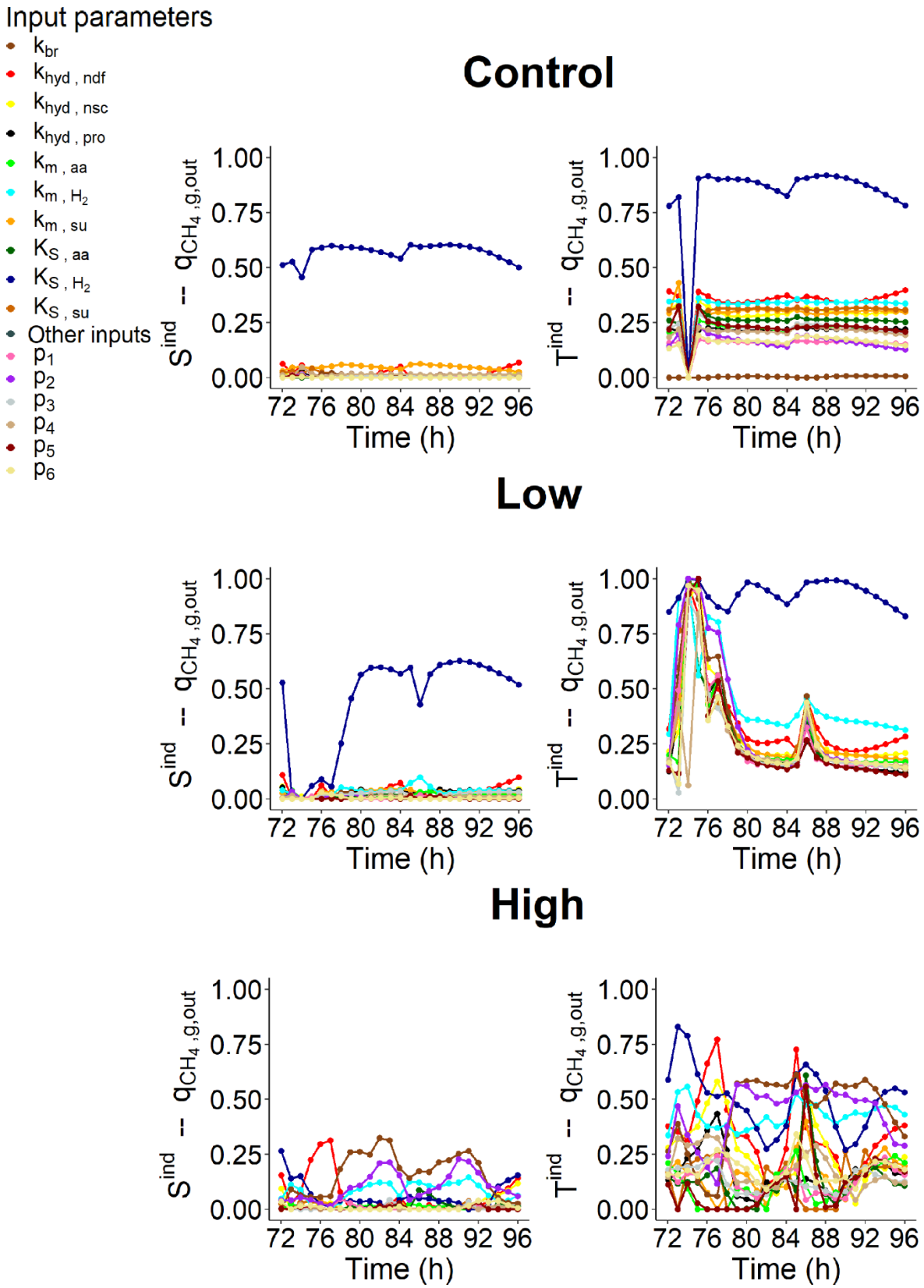

Figure 12. Independent first-order (S^{ind}) and total Sobol indices (T^{ind}) of the input parameters over time (h) computed for the 4th day of simulation of the rate of CH_4 production in gas phase ($q_{CH_4,g,out}$, mol/h) for the 3 dietary scenarios (control: 0% of *Asparagopsis taxiformis*, low treatment: 0.25% of *Asparagopsis taxiformis* and high treatment: 0.50% of *Asparagopsis taxiformis*).

592

The difference between $\mathrm{T_i^{ind}}$ and $\mathrm{S_i^{ind}}$ over time indicated that interactions between IPs had an important influence on its variation for the control and two AT treatments over the fermentation.

For control, the variability of $K_{\mathrm{S,H_2}}$ alone had a high contribution on the variation of $q_{\mathrm{CH_4,g,out}}$ ($\mathrm{S}_{K_{\mathrm{S,H_2}}}^{\mathrm{ind}}$ varying from 45 to 60%). The contribution of $K_{\mathrm{S,H_2}}$ increased over the fermentation when considering its influence via the interactions with other IPs over time ($\mathrm{T}_{K_{\mathrm{S,H_2}}}^{\mathrm{ind}}$ varying from 78 to 92%). The other IPs did not show any contribution due to their own variability ($\mathrm{S}_{i,\mathrm{i}\neq K_{\mathrm{S,H_2}}}^{\mathrm{ind}}$ c.a. 0). However, their independent total indices indicated that all the IPs interacted with $K_{\mathrm{S,H_2}}$ ($\mathrm{T_i^{ind}} \geq 10\%$), except k_{br} with $\mathrm{T}_{k_{\mathrm{br}}}^{\mathrm{ind}}$ c.a. 0 over the fermentation (which is obvious since there is not bromoform in the control). The influential contribution due to the interactions between IPs was mostly due to interactions of $K_{\mathrm{S,H_2}}$ with other IPs such as the fibers degradation ($k_{\mathrm{hyd,ndf}}$), the maximum utilization rate of hydrogen utilizers microbial group ($k_{\mathrm{m,H_2}}$), the microbial group of sugars utilizers ($K_{\mathrm{S,su}}$ and $k_{\mathrm{m,su}}$), the non-fibers degradation ($k_{\mathrm{hyd,nsc}}$) and the microbial group of amino acids utilizers ($K_{\mathrm{S,aa}}$) with on average $\mathrm{T}_{\mathrm{i,i}=k_{\mathrm{hyd,ndf}},k_{\mathrm{m,H_2}},K_{\mathrm{S,su}},k_{\mathrm{m,su}},k_{\mathrm{hyd,nsc}},K_{\mathrm{S,aa}}}^{\mathrm{ind}}$ higher than 25% over time.

For low AT treatment, $K_{\mathrm{S,H_2}}$ was the only IP contributing to $q_{\mathrm{CH_4,g,out}}$ variation via its own variability over time, similarly to the control. $\mathrm{S}_{K_{\mathrm{S,H_2}}}^{\mathrm{ind}}$ varied from 0 to 63% over the fermentation with a contribution lower than 10% from t = 73 to 77h, corresponding to the highest intake activity of the first feed distribution. During this time period, $q_{\mathrm{CH_4,g,out}}$ variation was only explained by the interactions between the 16 IPs, with $\mathrm{T_i^{ind}}$ higher than 80% for all the IPs for at least one time step during this time period. Similarly to the control, $K_{\mathrm{S,H_2}}$ also explained almost all the variability of $q_{\mathrm{CH_4,g,out}}$ over the fermentation when considering the contribution via the interactions with other IPs with $\mathrm{T}_{K_{\mathrm{S,H_2}}}^{\mathrm{ind}}$ varying from 82 to 100% over time. These interactions mainly included $k_{\mathrm{m,H_2}}$ and $k_{\mathrm{hyd,ndf}}$ with $\mathrm{T}_{k_{\mathrm{m,H_2}}}^{\mathrm{ind}} = 36\%$ and $\mathrm{T}_{k_{\mathrm{hyd,ndf}}}^{\mathrm{ind}} = 28\%$ on average over time.

For high AT treatment, $\mathrm{S_i^{ind}}$ was lower than 32% for all the IPs, indicating that the variation of $q_{\mathrm{CH_4,g,out}}$ was mainly due to the interactions between IPs. The IP with the most important individual contribution over the fermentation was $k_{\mathrm{hyd,ndf}}$ during the first feed distribution ($\mathrm{S}_{k_{\mathrm{hyd,ndf}}}^{\mathrm{ind}}$ varying from 22 to 31% from t = 75 to 77h) and at the end of the fermentation ($\mathrm{S}_{k_{\mathrm{hyd,ndf}}}^{\mathrm{ind}} = 14\%$ at t = 96h). Then, the contribution of other IPs such as k_{br} ($\mathrm{S}_{k_{\mathrm{br}}}^{\mathrm{ind}}$ varying from 14 to 32%), p_2 ($\mathrm{S}_{p_2}^{\mathrm{ind}}$ varying from 4 to 23%) and $k_{\mathrm{m,H_2}}$ ($\mathrm{S}_{k_{\mathrm{m,H_2}}}^{\mathrm{ind}}$ varying from 3 to 14%) was low in the middle of fermentation from t = 78 to 92h. Also, $K_{\mathrm{S,H_2}}$ showed the most important contribution at the beginning and end of the fermentation with $\mathrm{S}_{K_{\mathrm{S,H_2}}}^{\mathrm{ind}} = 26$ and 15% at t = 72 and 96h, respectively. When considering the interactions between IPs, their contribution increased significantly. All the IPs showed a non-negligible contribution (> 20%) for at least one time step, indicating that the 16 IPs were considered in the interactions contributing to $q_{\mathrm{CH_4,g,out}}$ variation. IP $K_{\mathrm{S,H_2}}$ contributed the most via its interactions with an average

difference between $\mathrm{T}^{\mathrm{ind}}_{K_{\mathrm{S,H_2}}}$ and $\mathrm{S}^{\mathrm{ind}}_{K_{\mathrm{S,H_2}}}$ over time of 42%. IP $k_{\mathrm{m,H_2}}$ also showed an important contribution throughout the fermentation via the interactions with other IPs with an average constant contribution of 34% over time. The third and fourth IPs contributed the most via the interactions were p_2 and k_{br}, respectively, with on average $\mathrm{T}^{\mathrm{ind}}_{p_2} - \mathrm{S}^{\mathrm{ind}}_{p_2} = 33\%$ and $\mathrm{T}^{\mathrm{ind}}_{k_{\mathrm{br}}} - \mathrm{S}^{\mathrm{ind}}_{k_{\mathrm{br}}} = 28\%$ over time. These contributions were more important in the middle of fermentation from t = 78 to 92h. Finally, $k_{\mathrm{hyd,ndf}}$ and $k_{\mathrm{hyd,nsc}}$ also showed a non-negligible contribution via the interactions with on average $\mathrm{T}^{\mathrm{ind}}_{k_{\mathrm{hyd,ndf}}} - \mathrm{S}^{\mathrm{ind}}_{k_{\mathrm{hyd,ndf}}} = 28\%$ and $\mathrm{T}^{\mathrm{ind}}_{k_{\mathrm{hyd,nsc}}} - \mathrm{S}^{\mathrm{ind}}_{k_{\mathrm{hyd,nsc}}} = 24\%$ over time.

3.2.2.2. Volatile fatty acids concentration

For VFA concentrations (s_{ac}, s_{bu} and s_{pr}, mol/L), the contribution of the interactions between IPs to their variation was lower than 20% (i.e. $\mathrm{T}^{\mathrm{ind}}_{\mathrm{i}} - \mathrm{S}^{\mathrm{ind}}_{\mathrm{i}} \leq 20\%$) for the 3 dietary scenarios studied, except for p_5 which described the fraction of glucose utilized to produce propionate and showed a strong influence on s_{ac}, s_{bu} and s_{pr} variation of the control with a maximum contribution of 60, 38 and 29%, respectively. For these 3 variables, the maximum contribution of p_5 via the interactions was reached at the end of the fermentation. Also, the interactions between $k_{\mathrm{m,H_2}}$ and other IPs showed a contribution of 24% and 19% to s_{ac} variation for low and high AT treatments, respectively.

3.3. Uncertainty analysis

Similarly to the full and independent Sobol indices, the uncertainty analysis of simulations computed for estimating the Shapley effects was displayed only for $q_{\mathrm{CH_4,g,out}}$. Simulations of VFA used for estimating the Shapley effects were associated with a low variability with a maximum CV of 0.08, 0.12 and 0.09 for s_{ac}, s_{bu} and s_{pr}, respectively.

Figure 13 displays the median and quantiles 10% and 90% over time of $q_{\mathrm{CH_4,g,out}}$ simulations computed using the IP sampling matrix and the calculated Shapley effects of the 3 dietary scenarios.

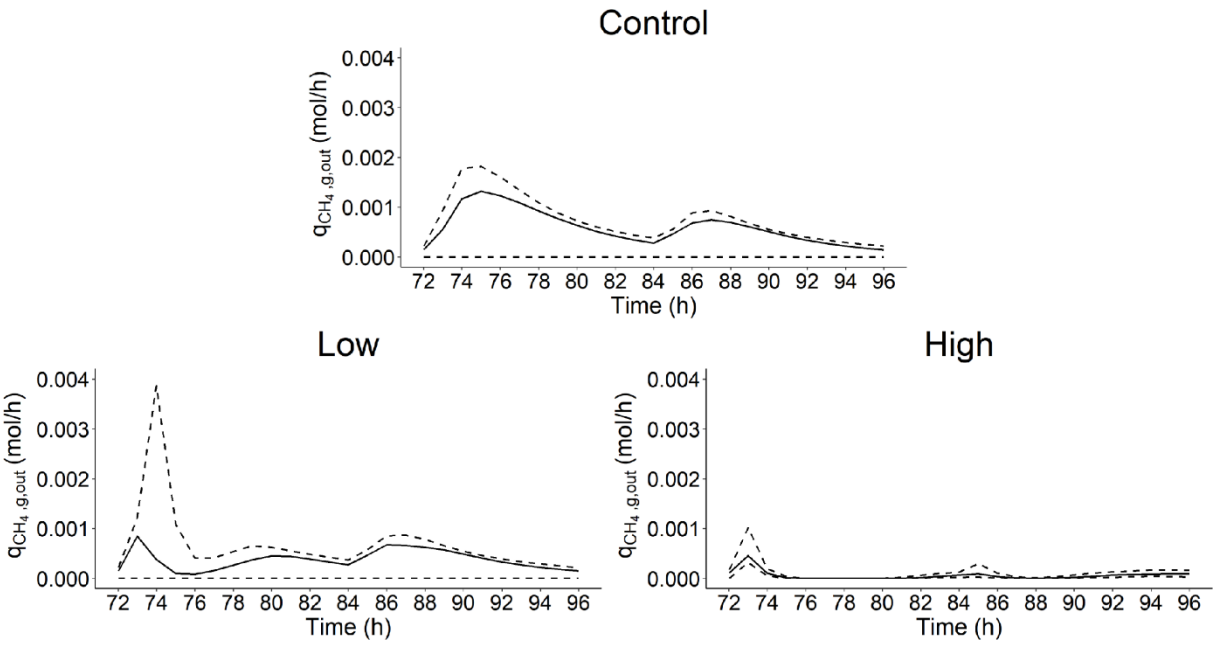

Figure 13. Median and 0.1 and 0.9 quantiles of the rate of methane production in gas phase ($q_{\mathrm{CH_4,g,out}}$, mol/h) over time (h) computed from the simulations used to calculate the Shapley effects for the 3 dietary scenarios (control: 0% of *Asparagopsis taxiformis*, low treatment: 0.25% of *Asparagopsis taxiformis* and high treatment: 0.50% of *Asparagopsis taxiformis*).

When not considering the 10% more extreme simulations, the CV highlighted that $q_{\mathrm{CH_4,g,out}}$ simulations showed a lower variability for low and high AT treatments with a median CV of 0.74 and 0.59, respectively. Whereas, the control showed a median CV of 0.78.

Moreover, Figure 14 highlighted that $q_{\mathrm{CH_4,g,out}}$ variability varied over time and that this variability was related to the dynamic of DMI (g/h).

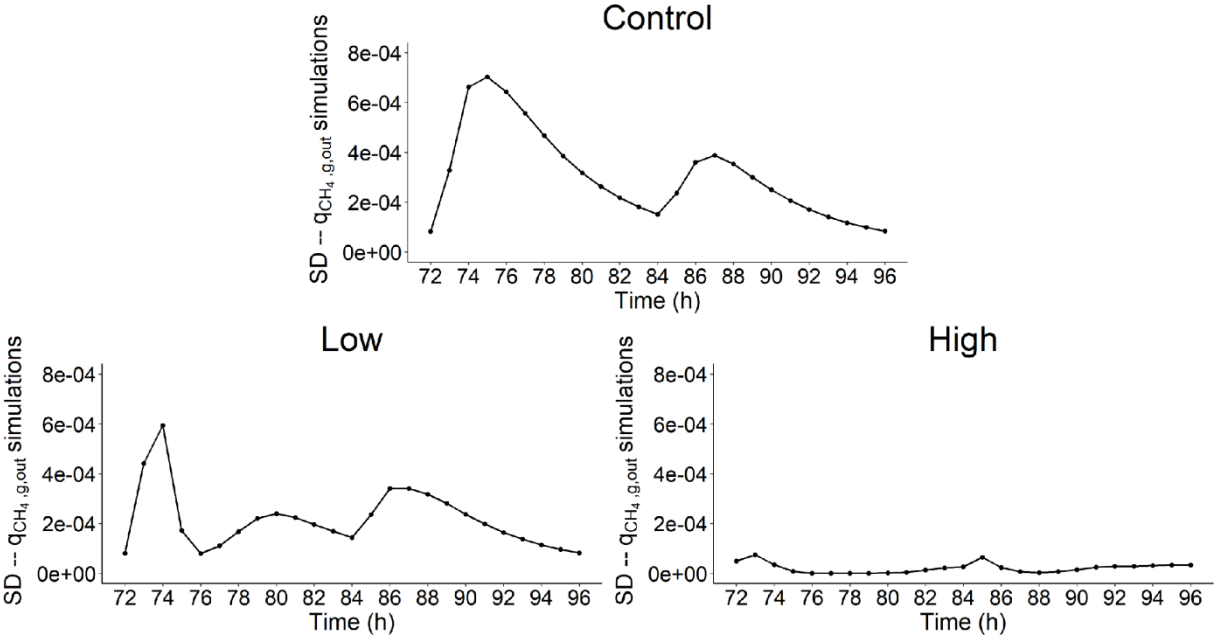

Figure 14. Standard deviation of the simulations of rate of methane production in gas phase ($q_{\mathrm{CH_4,g,out}}$, mol/h) over time (h) used to calculate the Shapley effects for the 3 dietary scenarios (control: 0% of *Asparagopsis taxiformis*, low treatment: 0.25% of *Asparagopsis taxiformis* and high treatment: 0.50% of *Asparagopsis taxiformis*).

The time periods associated with the highest intake activity (represented by the level of decay of the curve of Figure 2) were between 72 and 78h for the first feed distribution and 84 and 90h for the second feed distribution. The first feed distribution time period was systematically associated with the highest variability of $q_{\mathrm{CH_4,g,out}}$ simulations with a maximum SD of 7e-04 mol/h at t = 75h, 6e-04 mol/h at t = 74h and 7e-05 mol/h at t = 73h for control, and low and high AT treatments, respectively. This feed distribution represented 70% of the total DM. The second feed distribution, representing 30% of the total DM, was also associated with an important variability of $q_{\mathrm{CH_4,g,out}}$ simulations for the 3 dietary scenarios.

4. Discussion

4.1. Analysis of the simulations of the mechanistic model

4.1.1. Comparison with *in vitro* and *in vivo* studies

CH_4 reductions between AT treatments obtained with the mechanistic model were lower than those reported in *in vitro* and *in vivo* studies.

Chagas et al. (2019) indicated that the inclusion of AT (10 g/kg OM) decreased predicted *in vivo* CH_4 production (mL/g DM) of 99% under *in vitro* condition. Whereas, the RUSITEC of Roque et al. (2019) and the *in vitro* study of Romero et al. (2023b) reported reductions of CH_4

production (mL/g OM and mL, respectively) of 95% (with a 5% OM dose) and 97% (with a 2% DM dose), respectively.

Under *in vivo* conditions, Roque et al. (2021) tested AT doses similar to our simulations. This work reported *in vivo* CH_4 production (g/d) reduction of 32.7 and 51.9% between control, and low and high AT treatments, respectively. The model simulated a lower reduction for low AT treatment and a higher reduction for high AT treatment.

These results highlighted that some interactions occurring during the fermentation are not represented in the model (e.g. forage wall content might inhibit the effect of AT). Improving the model involves a finer representation of the interactions between feed characteristics and fermentation as discussed by Bannink et al. (2016).

4.1.2. Analysis of the behavior of VFA proportions

The behavior of VFA proportions dynamic between AT treatments simulated with the models was similar to that of *in vitro* studies. In Chagas et al. (2019), the AT treatment was associated with lower molar proportion of acetate (- 75%) and higher molar proportions of propionate and butyrate (+ 38% and + 47%, respectively). Moreover, the increase of the propionate to acetate ratio was highlighted in Roque et al. (2019) and Romero et al. (2023b). This highlights that the VFA dynamic behavior between AT treatment simulated by the model was consistent with the *in vitro* experiments.

4.2. Sensitivity analysis

4.2.1. General contribution of the input parameters

4.2.1.1. Rate of methane production

For the control and low AT treatment, all the variation of $q_{\mathrm{CH_4,g,out}}$ were explained by the action of the microbial group of hydrogen utilizers represented by the Monod constant $K_{\mathrm{S,H_2}}$. The dynamic of the impact of this microbial group was constant over time and slightly followed the dynamic of DMI.

Among all the polymer components describing the feed intake, microbes degrading the fibers with the kinetic $k_{\mathrm{hyd,ndf}}$ explained also a very low part of $q_{\mathrm{CH_4,g,out}}$ variation. It was also associated with a constant dynamic, following the dynamic of DMI.

The comparison of our results with the results of previous SA conducted on mechanistic models of rumen fermentation is not straightforward given the specific model strucutres and their mathematical formulation. Consequently, the model structure, and the variables and parameters considered in these models are different from those used in our representation, except for Merk et al. (2023) which conducted its SA on an adapted version of the model of Muñoz-Tamayo et al. (2021). However, considering our results in relation to those obtained in previous studies provides useful information to improve our knowledge of the whole picture of the rumen fermentation.

When no dose of AT was considered, Merk et al. (2023) also highlighted the impact of fibers degradation component on CH_4 production variation via the initial neutral detergent fiber concentration and $k_{\mathrm{hyd,ndf}}$. This is the initial condition of neutral detergent fiber that was largely associated with the highest contribution (= 43%) to CH_4 production variation. Its other influential IP for the control was related to the flux allocation parameter from glucose utilization to propionate production (λ_2). This last IP was not considered in our SA as we modified the flux allocation parameters in our model version.

The low AT treatment highlighted the low participation of IPs describing the kinetic of bromoform utilization (k_{br}) and the direct effect of bromoform on methanogenesis (p_2) to the variability of $q_{\mathrm{CH_4,g,out}}$, suggesting that the AT dose was too low to highlight a shift in the factors associated to microbial pathways impacting CH_4 production.

This shift was highlighted for high AT treatment. k_{br} and p_2 were associated with a high impact on CH_4 production in the middle of the fermentation, replacing a part of the variability explained by the hydrogen utilizers microbial group. However, the impact of $K_{\mathrm{S,H_2}}$ was still important over time, especially at the beginning and at the end of the fermentation. Other IPs associated with the direct (p_1) or indirect (p_4, p_5 and p_6) effect of bromoform on the fermentations were associated with a low influence on $q_{\mathrm{CH_4,g,out}}$ variation. This work highlighted that the use of AT to mitigate CH_4 production led to a shift in the factors associated to microbial pathways of the rumen fermentation impacting the CH_4 production.

In presence of a dose of AT (included at a 5% inclusion rate) , the high impact of IPs associated with bromoform concentration and the factor I_{br} on CH_4 production variation was also highlighted in Merk et al. (2023). The initial bromoform concentration and p_1 showed the highest contributions (= 46%) to CH_4 production variation. This study also mentioned the low but non-negligible impact (c.a. 10%) of IPs related to methanogen abundance, total microbial concentration and hydrogen utilizers microbial group represented by $k_{\mathrm{m,H_2}}$. This last IP showed also an influence on $q_{\mathrm{CH_4,g,out}}$ variation for high AT treatment in our work. Therefore, Merk et al. (2023) also identified a shift in the key factors driving CH_4 production variation in presence of AT.

For other references, the comparison of SA results is only valid for the control as other models did not consider AT treatments. Huhtanen et al. (2015) concluded that IPs associated with degradation kinetics of neutral detergent fiber had a strong influence on CH_4 predictions of Karoline. This factor was also identified as influential in our work but was not associated with a high influence. Fat and the degradation of starch and insoluble protein were the other factors associated with an influence on CH_4 production. Whereas, van Lingen et al. (2019) highlighted that IPs associated with the fractional passage rate for the solid and fluid fractions in the rumen and NADH oxidation rate explained 86% of CH_4 predictions variation of a modified version of the Dijkstra model. Our model does not include the different passage rates between solid and liquid fractions. Finally, Dougherty et al. (2017) found that influential IPs on daily CH_4 production predicted with the AusBeef model were associated with ruminal hydrogen balance and VFA production.

759 #### 4.2.1.2. Volatile fatty acids concentration

760 VFA concentration variation were highly impacted by fibers degradation represented by the
761 kinetic $k_{\mathrm{hyd,ndf}}$ for the control and two AT treatments. $k_{\mathrm{hyd,ndf}}$ was always associated with
762 the highest contribution for s_{ac}, s_{bu} and s_{pr} and the 3 dietary scenarios studied. This
763 contribution was very high (> 50%) for s_{ac} control, s_{bu} high AT treatment and s_{pr}. While, it
764 was intermediate (between 30 and 40% over the fermentation) for s_{ac} low and high AT
765 treatments, and s_{bu} control and low AT treatment. The dynamic of this influence was globally
766 constant over time slightly following the dynamic of DMI, except for s_{ac} low AT treatment
767 which showed a decrease during the first feed distribution. This result was expected as fiber
768 hydrolysis is the limiting step of the fermentation and VFA proportion. Morales et al., (2021)
769 studied the sensitivity of 19 IPs on VFA concentration predicted with Molly. It found that the
770 intercept used for rumen pH prediction was the only influential IP, explaining more than 79%
771 of the variation of acetate, butyrate and propionate concentration predictions of Molly. In this
772 study this result was expected as Molly is a whole animal model, which was not the case of
773 our model. No IPs related to rumen pH were considered in our SA, explaining that the selection
774 of this component was not possible in our case.
775 Hydrogen utilizers microbial group slightly impacted (< 30%) the variation of s_{ac} and s_{bu} for
776 low AT treatment with the 2 IPs representing this group ($K_{\mathrm{S,H_2}}$and $k_{\mathrm{m,H_2}}$). The influence of
777 these IPs was increasing at the beginning of the fermentation, constant in the middle of the
778 fermentation and decreasing at the end of the fermentation.
779 No shift of the factors associated to microbial pathways impacting VFA production was
780 highlighted when increasing the dose of AT. Moreover, IPs related to the direct effect of
781 bromoform on the fermentation (p_1 and p_2) did not contribute to VFA concentration variation.
782 This suggests that under the conditions evaluated AT had no impact on the biological
783 mechanisms responsible for VFA production in contrast with the one responsible for CH_4
784 production. However, AT supply does have an indirect effect on VFA production to its effect
785 on the lambdas and a variation was observed when considering the molar proportions of VFA
786 (Figure 7).
787 Furthermore, IPs associated with the functions describing the indirect effect of bromoform on
788 rumen fermentation and quantifying reactions driving flux allocation from glucose utilization
789 to acetate (λ_1 associated with p_3 and p_4) and propionate (λ_2 associated with p_5 and p_6)
790 production showed a low impact on VFA concentration variation under our conditions. IP p_3
791 was associated with an impact on s_{ac} and s_{bu} variation. This impact was highlighted for the
792 control and two AT treatments studied with a contribution decreasing at the beginning of the
793 fermentation and then increasing over time lower than 20% for control and low AT treatment
794 and of c.a. 25% for high AT treatment for s_{ac}. Whereas, the contribution over time was more
795 important for the control (c.a. 25%) than for the 2 AT treatments (<20%) for s_{bu} with the same
796 dynamic. p_4, the negative slope of λ_1, slightly impacted s_{ac} variation of high AT treatment
797 with a constant dynamic. Regarding λ_2, p_5 slightly impacted (<30%) s_{bu} and s_{pr} variation over
798 the fermentation for the 3 dietary scenarios with a dynamic slightly decreasing at the

beginning of the fermentation and then increasing over time, similarly to p_3. The positive slope p_6 did not contribute to VFA concentration variation.

4.2.2. Contribution of the interactions between the input parameters

In addition to the Shapley effects, full and independent Sobol indices allowed us to investigate if the influential IPs contributed through their own variability or through the variability generated by their dependence/correlation and/or their interactions with other IPs. This step was done as an academic exercise since, by construction, the model does not have dependency between IPs. However, the methodology here illustrated can be useful to address the dependency aspects in future model extensions.

4.2.2.1. Rate of methane production

First-order and total independent Sobol indices highlighted that interactions between IPs played an important role in the contribution of the IPs to $q_{\mathrm{CH_4,g,out}}$ variation for the control and AT treatments. This contribution was higher for AT treatments than for the control, with the highest contribution for low AT treatment. Merk et al. (2023) also identified the importance of the contribution due to the interactions between IPs for the AT treatment. However, no impact of the interactions was highlighted for the control.

The interactions between hydrogen utilizers microbial group via $K_{\mathrm{S,H_2}}$ and the other factors associated to microbial pathways of the rumen fermentation considered had an intermediate impact (~25%) on $q_{\mathrm{CH_4,g,out}}$ variation for the 3 dietary scenarios considered. Most of the time, these interactions included all the IPs, except k_{br} for the control.

The inclusion of all the IPs in the interactions impacting $q_{\mathrm{CH_4,g,out}}$ variation suggests that the model should be improved to better characterize the interactions. The incorporation of microbial genomic knowledge is expected to improve the representation of rumen microbial fermentation in mathematical models (Davoudkhani et al., 2024; Muñoz-Tamayo et al., 2023).

The first feed distribution of the low AT treatment showed that the variation of $q_{\mathrm{CH_4,g,out}}$ can also be only impacted by the interactions between IPs, highlighting the importance of quantifying the interactions between IPs in SA approaches used.

4.2.2.2. Volatile fatty acids concentration

The contribution due to the interactions was low for VFA concentration variation. Only p_5, the intercept of λ_2 which is related to propionate production, showed a high contribution via the interactions to VFA concentration variation for control.

Finally, the interactions did not affect the dynamic of the contribution over the fermentation for $q_{\mathrm{CH_4,g,out}}$ and VFA concentrations.

4.3. Uncertainty analysis

The uncertainty of $q_{\mathrm{CH_4,g,out}}$ and VFA concentration simulations used to compute the Shapley effects was assessed by studying the variability over time of these simulations.

4.3.1. Rate of methane production

The simulations of $q_{\mathrm{CH_4,g,out}}$ computed by exploring the variability of 6 factors associated to microbial pathways of the rumen fermentation (fiber carbohydrates, non-fiber carbohydrates, proteins, glucose utilizers, amino acids utilizers, hydrogen utilizers) and 4 factors of the effect of bromoform on the fermentation (s_{br}, I_{br}, λ_1 and λ_2) showed a high range of variation for the 3 dietary scenarios.

SA results indicated that the variability of $q_{\mathrm{CH_4,g,out}}$ simulations was only explained by the variation of hydrogen utilizers microbial group via $K_{\mathrm{S,H_2}}$ (alone and in interaction with other factors) for control and low AT treatment. Whereas, the variability of $K_{\mathrm{S,H_2}}$ explained an important part, but also with the variability of other factors, of $q_{\mathrm{CH_4,g,out}}$ simulation variability for high AT treatment. This suggests that reducing uncertainty associated with $q_{\mathrm{CH_4,g,out}}$ predictions involves to reduce the uncertainty of IPs describing the activity of the hydrogen utilizers microbial group. A way to achieve that is to increase the information available for estimating the variability of parameters describing this microbial group, involving an improvement of our knowledge of it. Finally, when comparing control and AT treatments, $q_{\mathrm{CH_4,g,out}}$ simulation variability was more important for the control than for low and high AT treatments. This indicates that the shift and increase of factors explaining the variation of $q_{\mathrm{CH_4,g,out}}$ did not lead to an increase of simulation variability, especially for high AT treatment. Merk et al., (2023) found a different result, computing a CV of 0.23 against 1.22 for simulations associated with control and AT treatment, respectively. However, the range of variation of IPs explored in our study led to outlier simulation for AT treatments. For instance, an IP simulation scenario led to $q_{\mathrm{CH_4,g,out}}$ values of 96 and 0.07 mol/h at t = 74 and 73h for low and high AT treatments, respectively. These outliers were not identified for the control. This suggests that some of the range of variation explored for $K_{\mathrm{S,H_2}}$, $k_{\mathrm{m,H_2}}$, p_2 and k_{br} was not appropriate when considering AT treatments.

The dynamic of simulation variability was related to the dynamic of DMI, increasing during the high intake activity period of both feed distributions and decreasing at the end of it. The highest period of variability was associated with the first feed distribution, which corresponded to 70% of the total DM. These results go in line with model developments predicting CH_4 with dynamic data DMI as single predictor (Muñoz-Tamayo et al., 2019, 2022).

4.3.2. Volatile fatty acids concentration

VFA concentrations were associated with much less variability than $q_{\mathrm{CH_4,g,out}}$, suggesting that these variables are less sensitive to the variation of factors associated to microbial pathways

involved in the rumen fermentation analyzed here. Perhaps the consideration of other parameters such as the yield factors would lead to a higher variability of VFA simulations. The variability of these variables was only explained by the individual variability of the kinetic of fibers degradation $k_{\mathrm{hyd,ndf}}$. This suggests that the uncertainty related to $k_{\mathrm{hyd,ndf}}$ measurements generates a low uncertainty on VFA concentrations.

Similarly to $q_{\mathrm{CH_4,g,out}}$, the dynamic of the variability of VFA concentration simulations was related to the dynamic of DMI. This variability increased during the high intake activity periods of the first and second feed distributions, with the highest variability reached for the first feed distribution, and decreased at the end of both feed distributions.

4.4. Limitations and perspectives of methods

4.4.1. Sensitivity analysis approaches

The computation of the Shapley effects allowed to identify the influential and non-influential IPs on the variation of $q_{\mathrm{CH_4,g,out}}$ and VFA concentration. The use of sensitivity indices for this purpose is becoming increasingly widespread in animal science and our work contributes to the integration of SA in animal modeling. For instance, Merk et al. (2023) conducted local and global SA for identifying key drivers of CH_4 production with or without AT.

The main originality of our work is the computation of SI over time, leading to a dynamic interpretation of the impact of key drivers on CH_4 and VFA variation. A second originality is the proposition of an approach allowing to discriminate the nature of the contribution of IPs to output variable variation. Although, considering the contribution due to the dependence/correlation between IPs was not relevant in our case study, this work proposes a first methodology to handle this kind of contribution in the case of development of more complex models involving dependent or correlated IPs.

Our study used simulation conditions based on RUSITEC *in vitro* experiments. Future work can use our SA framework to identify useful sampling times and experimental conditions to provide informative data for model refinement in the context of optimal experiment design for parameter estimation.

Regarding our SA results, it is important to mention that they are inherently linked to the representation of the rumen fermentation considered in our case study.

4.4.2. Uncertainty analysis

The *in silico* framework used for the SA shows that the factors associated to microbial pathways modeled in our case study mainly impacted CH_4 prediction uncertainty. This suggests that an improvement in the range of variation of parameters associated with the methanogenesis should lead to a reduction of the uncertainty associated with model predictions. The high AT treatment also showed that the parameters associated with the bromoform effect on the fermentation impacted negatively the prediction uncertainty. These

suggestions should be carefully interpreted because limited by the low information available on the numerical values of parameters of the equations representing the rumen fermentation.

5. Conclusions

A dynamic sensitivity analysis of a model describing the effect of bromoform (via *Asparagopsis taxiformis*) on rumen fermentation under *in vitro* continuous condition was conducted. The hydrogen utilizers microbial group was identified as the key factor explaining methane variation over time for the control and low dose treatments. This factor was associated with the microbial methanogenesis. The high AT dose treatment showed a shift in the factors associated to microbial pathways explaining methane variation, highlighting the emergence of parameters associated with bromoform concentration and direct effect of bromoform on methanogenesis. The interactions between parameters played a role in these contributions. Moreover, the individual variability of kinetic of fibers degradation explained most of the VFA variation. The uncertainty analysis of simulations computed for SA suggested that reducing the uncertainty of the parameters associated to the kinetics of hydrogen utilizers microbial group should lead to a reduction of model prediction uncertainty. Our work showed that implementing dynamic sensitivity analysis is a promising approach to improve our understanding of mechanisms involved in the rumen fermentation and can help to design optimal experiments assessing methane mitigation strategies.

6. Declarations

Funding

Paul Blondiaux is funded with a scholarship from the doctoral school ABIES (AgroParisTech, France) and from the INRAE PHASE department (France).

Availability of data and material

The scripts for the model simulation and SA are available at Blondiaux (2024)

Competing interests

The authors declare that they comply with the PCI rule of having no financial conflicts of interest in relation to the content of the article. The authors declare the following non-financial conflict of interest: Rafael Muñoz-Tamayo is member of the managing board of PCI Animal Science and recommender of PCI Microbiology.

CRediT Author contributions

Paul Blondiaux: Conceptualization, Data curation, Formal Analysis, Investigation, Methodology, Software, Writing – original draft

Tristan Senga Kiessé: Conceptualization, Funding acquisition, Methodology, Supervision, Writing – review & editing

Maguy Eugène: Conceptualization, Funding acquisition, Methodology, Supervision, Writing – review & editing

Rafael Muñoz-Tamayo: Conceptualization, Funding acquisition, Investigation, Methodology, Project administration, Software, Supervision, Writing – review & editing

7. References

Aluwong, T., Wuyep, P., Allam, L., 2011. Livestock-environment interactions: Methane emissions from ruminants. African J. Biotechnol. 10, 1265–1269. https://doi.org/10.4314/AJB.V10I8

Arndt, C., Hristov, A.N., Price, W.J., McClelland, S.C., Pelaez, A.M., Cueva, S.F., Oh, J., Dijkstra, J., Bannink, A., Bayat, A.R., Crompton, L.A., Eugéne, M.A., Enahoro, D., Kebreab, E., Kreuzer, M., McGee, M., Martin, C., Newbold, C.J., Reynolds, C.K., Schwarm, A., Shingfield, K.J., Veneman, J.B., Yáñez-Ruiz, D.R., Yu, Z., 2022. Full adoption of the most effective strategies to mitigate methane emissions by ruminants can help meet the 1.5 °C target by 2030 but not 2050. Proc. Natl. Acad. Sci. U. S. A. 119. https://doi.org/10.1073/PNAS.2111294119/-/DCSUPPLEMENTAL

Baldwin, R.L., Thornley, J.H.M., Beever, D.E., 1987. Metabolism of the lactating cow: II. Digestive elements of a mechanistic model. J. Dairy Res. 54. https://doi.org/10.1017/s0022029900025231

Bannink, A., Kogut, J., Dijkstra, J., France, J., Kebreab, E., Van Vuuren, A.M., Tamminga, S., 2006. Estimation of the stoichiometry of volatile fatty acid production in the rumen of lactating cows. J. Theor. Biol. 238, 36–51. https://doi.org/10.1016/j.jtbi.2005.05.026

Bannink, A., van Lingen, H.J., Ellis, J.L., France, J., Dijkstra, J., 2016. The contribution of mathematical modeling to understanding dynamic aspects of rumen metabolism. Front. Microbiol. 7, 166675. https://doi.org/10.3389/FMICB.2016.01820/BIBTEX

Batstone, D.J., Keller, J., Angelidaki, I., Kalyuzhnyi, S. V., Pavlostathis, S.G., Rozzi, A., Sanders, W.T., Siegrist, H., Vavilin, V.A., 2002. The IWA Anaerobic Digestion Model No 1 (ADM1). Water Sci. Technol. 45. https://doi.org/10.2166/wst.2002.0292

Bayat, A.R., Rinne, M., Kuoppala, K., Ahvenjärvi, S., Huhtanen, P., 2011. Ruminal large and small particle kinetics in dairy cows fed primary growth and regrowth grass silages harvested at two stages of growth. Anim. Feed Sci. Technol. 165, 51–60. https://doi.org/10.1016/j.anifeedsci.2011.02.018

Beauchemin, K.A., Ungerfeld, E.M., Eckard, R.J., Wang, M., 2020. Review: Fifty years of research on rumen methanogenesis: lessons learned and future challenges for mitigation. Animal 14, s2–s16. https://doi.org/10.1017/S1751731119003100

Belanche, A., Newbold, C.J., Lin, W., Stevens, P.R., Kingston-Smith, A.H., 2017. A systems biology approach reveals differences in the dynamics of colonization and degradation of grass vs. Hay by rumen microbes with minor effects of vitamin E supplementation. Front. Microbiol. 8, 1–18. https://doi.org/10.3389/fmicb.2017.01456

Benchaar, C., Rivest, J., Pomar, C., Chiquette, J., 1997. Prediction of Methane Production from Dairy Cows Using Existing Mechanistic Models and Regression Equations 1. J. Anim. Sci 76, 617–627.

Bertrand Iooss, A., Da Veiga, S., Janon, A., Pujol, G., contribu-tions from Baptiste Broto, with, Boumhaout, K., Clouvel, L., De-lage, T., El Amri, R., Fruth, J., Gilquin, L., Guillaume, J., Herin, M., Il Idrissi, M., Le Gratiet, L., Lemaitre, P., Marrel, A., Mey-naoui, A., Nelson, B.L., Monari, F., Oomen, R., Rakovec, O., Ramos, B., Rous-tant, O., Sarazin, G., Song, E., Staum, J., Sueur, R., Touati, T., Verges, V., Weber, F., 2023. Package "sensitivity" Title Global Sensitivity Analysis of Model Outputs.

Blondiaux, P., 2024. Implementation of a dynamic sensitivity analysis of a mathematical model describing the effect of the macroalgae Asparagopsis taxiformis on rumen fermentation and methane production under in vitro continuous conditions. https://doi.org/10.5281/ZENODO.12167243

Blondiaux, P., Senga Kiessé, T., Eugène, M., Muñoz-Tamayo, R., 2022. 20. Sensitivity analysis of a mechanistic model of the rumen in-vitro fermentation: Study of the impact of 3 sampling methods on Sobol indices of accuracy. Anim. - Sci. Proc. 13, 532–533. https://doi.org/10.1016/J.ANSCIP.2022.07.411

Castro, J., Gómez, D., Tejada, J., 2009. Polynomial calculation of the Shapley value based on sampling. Comput. Oper. Res. 36. https://doi.org/10.1016/j.cor.2008.04.004

Chagas, J.C., Ramin, M., Krizsan, S.J., 2019. In Vitro Evaluation of Different Dietary Methane Mitigation Strategies. Animals 9, 1120. https://doi.org/10.3390/ani9121120

Chapoutot, P., Dorléans, M., Sauvant, D., 2010. Études des cinétiques de dégradation dans le rumen des constituants pariétaux des aliments concentrés et coproduits agroindustriels. INRAE Prod. Anim. 23, 285–304. https://doi.org/10.20870/PRODUCTIONS-ANIMALES.2010.23.3.3309

CITEPA, 2023. Gaz à effet de serre et polluants atmosphériques. Bilan des émissions en France de 1990 à 2022.

Danfær, A., Huhtanen, P., Udén, P., Sveinbjörnsson, J., Volden, H., 2006. The nordic dairy cow model, karoline - description. Nutr. Dig. Util. Farm Anim. Model. Approaches 383–406. https://doi.org/10.1079/9781845930059.0383

Davoudkhani, M., Rubino, F., Creevey, C.J., Ahvenjärvi, S., Bayat, A.R., Tapio, I., Belanche, A., Muñoz-Tamayo, R., 2024. Integrating microbial abundance time series with fermentation dynamics of the rumen microbiome via mathematical modelling. PLoS One 19, e0298930. https://doi.org/10.1371/JOURNAL.PONE.0298930

Dijkstra, J., Neal, H.D.S.C., Beever, D.E., France, J., 1992. Simulation of nutrient digestion, absorption and outflow in the rumen: Model description. J. Nutr. 122. https://doi.org/10.1093/jn/122.11.2239

Dougherty, H.C., Kebreab, E., Evered, M., Little, B.A., Ingham, A.B., Nolan, J. V., Hegarty, R.S., Pacheco, D., Mcphee, M.J., 2017. The AusBeef model for beef production: II. sensitivity analysis. J. Agric. Sci. 155. https://doi.org/10.1017/S0021859617000430

Faivre, R., Iooss, B., Mahévas, S., Makowski, D., Monod, H., 2013. Analyse de sensibilité et exploration de modèles : Application aux sciences de la nature et de l'environnement 1–352.

Fao, 2017. Livestock solutions for climate change.

Homma, T., Saltelli, A., 1996. Importance measures in global sensitivity analysis of nonlinear models. Reliab. Eng. Syst. Saf. 52. https://doi.org/10.1016/0951-8320(96)00002-6

Hristov, A.N., Oh, J., Firkins, J.L., Dijkstra, J., Kebreab, E., Waghorn, G., Makkar, # H P S, Adesogan, ‖ A T, Yang, ¶ W, Lee, C., Gerber‖, P.J., Henderson‖, B., Tricarico, J.M., 2013. SPECIAL TOPICS-Mitigation of methane and nitrous oxide emissions from animal operations: I. A review of enteric methane mitigation options 1. J. Anim. Sci 91, 5045–

5069. https://doi.org/10.2527/jas2013-6583
Huhtanen, P., Ramin, M., Udén, P., 2015. Nordic dairy cow model Karoline in predicting methane emissions: 1. Model description and sensitivity analysis. Livest. Sci. 178. https://doi.org/10.1016/j.livsci.2015.05.009
Iooss, B., Lemaître, P., 2015. A review on global sensitivity analysis methods. Oper. Res. Comput. Sci. Interfaces Ser. 59, 101–122. https://doi.org/10.1007/978-1-4899-7547-8_5/COVER
Iooss, B., Prieur, C., 2019. Shapley effects for sensitivity analysis with correlated inputs: Comparisons with sobol' indices, numerical estimation and applications. Int. J. Uncertain. Quantif. 9. https://doi.org/10.1615/Int.J.UncertaintyQuantification.2019028372
IPCC, 2022. IPCC, 2018: Global Warming of 1.5°C. Cambridge University Press. https://doi.org/10.1017/9781009157940
Kinley, R.D., De Nys, R., Vucko, M.J., MacHado, L., Tomkins, N.W., 2016. The red macroalgae Asparagopsis taxiformis is a potent natural antimethanogenic that reduces methane production during in vitro fermentation with rumen fluid. Anim. Prod. Sci. 56, 282–289. https://doi.org/10.1071/AN15576
Kinley, R.D., Martinez-Fernandez, G., Matthews, M.K., De Nys, R., Magnusson, M., Tomkins, N.W., 2020. Mitigating the carbon footprint and improving productivity of ruminant livestock agriculture using a red seaweed. https://doi.org/10.1016/j.jclepro.2020.120836
Kucherenko, S., Tarantola, S., Annoni, P., 2012. Estimation of global sensitivity indices for models with dependent variables. Comput. Phys. Commun. 183. https://doi.org/10.1016/j.cpc.2011.12.020
Lescoat, P., Sauvant, D., 1995. Development of a mechanistic model for rumen digestion validated using the duodenal flux of amino acids.
Li, X., Norman, H.C., Kinley, R.D., Laurence, M., Wilmot, M., Bender, H., De Nys, R., Tomkins, N., 2016. Asparagopsis taxiformis decreases enteric methane production from sheep. Anim. Prod. Sci. 58, 681–688. https://doi.org/10.1071/AN15883
Machado, L., Magnusson, M., Paul, N.A., De Nys, R., Tomkins, N., 2014. Effects of Marine and Freshwater Macroalgae on In Vitro Total Gas and Methane Production. PLoS One 9, e85289. https://doi.org/10.1371/JOURNAL.PONE.0085289
Machado, L., Magnusson, M., Paul, N.A., Kinley, R., de Nys, R., Tomkins, N., 2016. Dose-response effects of Asparagopsis taxiformis and Oedogonium sp. on in vitro fermentation and methane production. J. Appl. Phycol. 28, 1443–1452. https://doi.org/10.1007/s10811-015-0639-9
Mara, T.A., Tarantola, S., 2012. Variance-based sensitivity indices for models with dependent inputs, in: Reliability Engineering and System Safety. https://doi.org/10.1016/j.ress.2011.08.008
Mara, T.A., Tarantola, S., Annoni, P., 2015. Non-parametric methods for global sensitivity analysis of model output with dependent inputs. Environ. Model. Softw. 72. https://doi.org/10.1016/j.envsoft.2015.07.010
Mcgrath, J., Duval, S.M., Tamassia, L.F.M., Kindermann, M., Stemmler, R.T., De Gouvea, V.N., Acedo, T.S., Immig, I., Williams, S.N., Celi, P., 2017. Nutritional strategies in ruminants: A lifetime approach. https://doi.org/10.1016/j.rvsc.2017.09.011
Merk, K., Link, K.G., Guy, R.D., Hess, M., 2023. Sensitivity analysis of a mechanistic model of rumen fermentation and methane production by rumen microbiota in the presence of

Asparagopsis taxiformis. bioRxiv 2023.11.30.569127. https://doi.org/10.1101/2023.11.30.569127

Mills, J.A.N., Crompton, L.A., Ellis, J.L., Dijkstra, J., Bannink, A., Hook, S., Benchaar, C., France, J., 2014. A dynamic mechanistic model of lactic acid metabolism in the rumen. J. Dairy Sci. 97, 2398–2414. https://doi.org/10.3168/JDS.2013-7582

Morales, A.G., Vibart, R.E., Li, M.M., Jonker, A., Pacheco, D., Hanigan, M.D., 2021. Evaluation of Molly model predictions of ruminal fermentation, nutrient digestion, and performance by dairy cows consuming ryegrass-based diets. J. Dairy Sci. 104, 9676–9702. https://doi.org/10.3168/JDS.2020-19740

Morgavi, D.P., Cantalapiedra-Hijar, G., Eugène, M., Martin, C., Noziere, P., Popova, M., Ortigues-Marty, I., Muñoz-Tamayo, R., Ungerfeld, E.M., 2023. Review: Reducing enteric methane emissions improves energy metabolism in livestock: is the tenet right? animal 17, 100830. https://doi.org/10.1016/J.ANIMAL.2023.100830

Morgavi, D.P., Forano, E., Martin, C., Newbold, C.J., 2010. Microbial ecosystem and methanogenesis in ruminants. Animal 4, 1024–1036. https://doi.org/10.1017/S1751731110000546

Mosey, F.E., 1983. Mathematical Modelling of the Anaerobic Digestion Process: Regulatory Mechanisms for the Formation of Short-Chain Volatile Acids from Glucose. Water Sci. Technol. 15, 209–232. https://doi.org/10.2166/WST.1983.0168

Muñoz-Tamayo, R., 2020. Implementation of a mathematical model predicting the impact of Asparagopsis taxiformis supply on in vitro rumen microbial fermentation and methane production. https://doi.org/10.5281/ZENODO.11239148

Muñoz-Tamayo, R., Chagas, J.C., Ramin, M., 2021a. Understanding the mechanisms behind natural bioactive compounds that can potentially reduce methane production in anaerobic conditions. A case study of Asparagopsis taxiformis. Peer Community Anim. Sci. 1, 100006. https://doi.org/10.24072/PCI.ANIMSCI.100006

Muñoz-Tamayo, R., Chagas, J.C., Ramin, M., Krizsan, S.J., 2021b. Modelling the impact of the macroalgae Asparagopsis taxiformis on rumen microbial fermentation and methane production. Peer Community J. 1. https://doi.org/10.24072/pcjournal.11

Muñoz-Tamayo, R., Davoudkhani, M., Fakih, I., Robles-Rodriguez, C.E., Rubino, F., Creevey, C.J., Forano, E., 2023. Review: Towards the next-generation models of the rumen microbiome for enhancing predictive power and guiding sustainable production strategies. animal 17, 100984. https://doi.org/10.1016/J.ANIMAL.2023.100984

Muñoz-Tamayo, R., Giger-Reverdin, S., Sauvant, D., 2016. Mechanistic modelling of in vitro fermentation and methane production by rumen microbiota. Anim. Feed Sci. Technol. 220. https://doi.org/10.1016/j.anifeedsci.2016.07.005

Muñoz-Tamayo, R., Ramírez Agudelo, J.F., Dewhurst, R.J., Miller, G., Vernon, T., Kettle, H., 2019. A parsimonious software sensor for estimating the individual dynamic pattern of methane emissions from cattle. animal 13, 1180–1187. https://doi.org/10.1017/S1751731118002550

Muñoz-Tamayo, R., Ruiz, B., Blavy, P., Giger-Reverdin, S., Sauvant, D., Williams, S.R.O., Moate, P.J., 2022. Predicting the dynamics of enteric methane emissions based on intake kinetic patterns in dairy cows fed diets containing either wheat or corn animal-open space. https://doi.org/10.1016/j.anopes.2021.100003

Nagorcka, B.N., Gordon, G.L.R., Dynes, R.A., Mcnamara, J.P., France, J., Beever, D.E., 2000. Towards a more accurate representation of fermentation in mathematical models of the rumen. Model. Nutr. Util. farm Anim. 37–48.

https://doi.org/10.1079/9780851994499.0037
Owen, A.B., 2014. Sobol' indices and shapley value. SIAM-ASA J. Uncertain. Quantif. 2. https://doi.org/10.1137/130936233
Pellerin, S., Bamière, L., Angers, D., Béline, F., Benoît, M., Butault, J.-P., Chenu, C., Colnenne-David, C., de Cara, S., Delame, N., Doreau, M., Dupraz, P., Faverdin, P., Garcia-Launay, F., Hassouna, M., Hénault, C., Jeuffroy, M.-H., Klumpp, K., Metay, A., Moran, D., Recous, S., Samson, E., Savini, I., Pardon, L., 2013. QUELLE CONTRIBUTION DE L'AGRICULTURE FRANÇAISE À LA RÉDUCTION DES ÉMISSIONS DE GAZ À EFFET DE SERRE ? POTENTIEL D'ATTÉNUATION ET COÛT DE DIX ACTIONS TECHNIQUES Synthèse du rapport de l' étude réalisée par l'INRA pour le compte de l' ADEME, du MAAF et du M.
Puy, A., Piano, S. Lo, Saltelli, A., Levin, S.A., 2022. **sensobol** : An *R* Package to Compute Variance-Based Sensitivity Indices. J. Stat. Softw. 102. https://doi.org/10.18637/jss.v102.i05
Romero, Pedro, Belanche, A., Jiménez, E., Hueso, R., Ramos-Morales, E., Salwen, J.K., Kebreab, E., Yáñez-Ruiz, D.R., 2023. Rumen microbial degradation of bromoform from red seaweed (Asparagopsis taxiformis) and the impact on rumen fermentation and methanogenic archaea. J. Anim. Sci. Biotechnol. 2023 141 14, 1–15. https://doi.org/10.1186/S40104-023-00935-Z
Romero, P., Huang, R., Jiménez, E., Palma-Hidalgo, J.M., Ungerfeld, E.M., Popova, M., Morgavi, D.P., Belanche, A., Yáñez-Ruiz, D.R., 2023. Evaluating the effect of phenolic compounds as hydrogen acceptors when ruminal methanogenesis is inhibited in vitro – Part 2. Dairy goats. animal 17, 100789. https://doi.org/10.1016/J.ANIMAL.2023.100789
Roque, B.M., Brooke, C.G., Ladau, J., Polley, T., Marsh, L.J., Najafi, N., Pandey, P., Singh, L., Kinley, R., Salwen, J.K., Eloe-Fadrosh, E., Kebreab, E., Hess, M., 2019. Effect of the macroalgae Asparagopsis taxiformis on methane production and rumen microbiome assemblage. Anim. Microbiome 1:3. https://doi.org/10.1186/s42523-019-0004-4
Roque, B.M., Venegas, M., Kinley, R.D., De Nys, R., Duarte, T.L., Yang, X., Kebreab, E., 2021. Red seaweed (Asparagopsis taxiformis) supplementation reduces enteric methane by over 80 percent in beef steers. PLoS One 16, e0247820. https://doi.org/10.1371/JOURNAL.PONE.0247820
Saltelli, A., Ratto, M., Andres, T., Campolongo, F., Cariboni, J., Gatelli, D., Saisana, M., Tarantola, S., 2008. Global sensitivity analysis: The primer. Glob. Sensit. Anal. Prim. 1–292. https://doi.org/10.1002/9780470725184
Saltelli, A., Ratto, M., Tarantola, S., Campolongo, F., 2005. Sensitivity analysis for chemical models. Chem. Rev. 105, 2811–2827. https://doi.org/10.1021/CR040659D
Serment, A., Giger-Reverdin, S., Schmidely, P., Dhumez, O., Broudiscou, L.P., Sauvant, D., 2016. In vitro fermentation of total mixed diets differing in concentrate proportion: Relative effects of inocula and substrates. J. Sci. Food Agric. 96, 160–168. https://doi.org/10.1002/JSFA.7076
Serment, A., Sauvant, D., 2011. A mechanistic model of pH and gas exchanges in the rumen and its in vitro application. Model. Nutr. Dig. Util. farm Anim. 148–157. https://doi.org/10.3920/978-90-8686-712-7_16
Shapley, L.S., 1953. A Value for n-person Games. Contributions to the Theory of Games. Ann. Math. Stud. 28.
Sobol, I.M., 1993. Sensitivity analysis for non-linear mathematical models. Math. Model. Comput. Exp. 1.
Song, E., Nelson, B.L., Staum, J., 2016. Shapley effects for global sensitivity analysis: Theory

and computation. SIAM-ASA J. Uncertain. Quantif. 4. https://doi.org/10.1137/15M1048070

Stefenoni, H.A., Räisänen, S.E., Cueva, S.F., Wasson, D.E., Lage, C.F.A., Melgar, A., Fetter, M.E., Smith, P., Hennessy, M., Vecchiarelli, B., Bender, J., Pitta, D., Cantrell, C.L., Yarish, C., Hristov, A.N., 2021. Effects of the macroalga Asparagopsis taxiformis and oregano leaves on methane emission, rumen fermentation, and lactational performance of dairy cows. J. Dairy Sci. 104, 4157–4173. https://doi.org/10.3168/JDS.2020-19686

Tedeschi, L.O., Cavalcanti, L.F.L., Fonseca, M.A., Herrero, M., Thornton, P.K., 2014. The evolution and evaluation of dairy cattle models for predicting milk production: An agricultural model intercomparison and improvement project (AgMIP) for livestock. Anim. Prod. Sci. 54, 2052–2067. https://doi.org/10.1071/AN14620

Terry, S.A., Krüger, A.M., Lima, P.M.T., Gruninger, R.J., Abbott, D.W., Beauchemin, K.A., 2023. Evaluation of Rumen Fermentation and Microbial Adaptation to Three Red Seaweeds Using the Rumen Simulation Technique. Anim. 2023, Vol. 13, Page 1643 13, 1643. https://doi.org/10.3390/ANI13101643

Torres, M.G., Soriano, R., Peralta, J.J., Alejos, J.I., Sánchez, P., Arias, L., Campos, R.G., Almaraz, I., 2020. Challenges of livestock: climate change, animal welfare and agroforestry. Large Anim. Rev. 26, 39–45.

van Lingen, H.J., Fadel, J.G., Moraes, L.E., Bannink, A., Dijkstra, J., 2019. Bayesian mechanistic modeling of thermodynamically controlled volatile fatty acid, hydrogen and methane production in the bovine rumen. J. Theor. Biol. 480. https://doi.org/10.1016/j.jtbi.2019.08.008

Xu, C., 2013. Decoupling correlated and uncorrelated parametric uncertainty contributions for nonlinear models. https://doi.org/10.1016/j.apm.2013.05.036

Xu, C., Zdzislaw Gertner, G., 2008. Uncertainty and sensitivity analysis for models with correlated parameters. Reliab. Eng. Syst. Saf. 93, 1563–1573. https://doi.org/10.1016/j.ress.2007.06.003